Polarization transfer solid-state NMR for studying soft matter: From surfactants to the stratum corneum

Nowacka, Agnieszka

2012

Total number of authors:
1

Polarization transfer solid-state NMR for studying soft matter:
From surfactants to the stratum corneum

Agnieszka Nowacka

LUND
UNIVERSITY

Doctoral Thesis in Physical Chemistry

This thesis will be publicly defended at 10.30 on Friday the 1st of June 2012 in lecture hall C, Kemicentrum.

The faculty opponent is Professor Dominique Massiot, CEMTHI, Orléans, France.

Organization		Document name	
Lund University		*Doctoral dissertation*	
		Date of issue	
		June 1st, 2012	
Author		Sponsoring organization	
Agnieszka Nowacka		*Swedish Research Council (VR)*	

Title and subtitle

Polarization transfer solid-state NMR for studying soft matter:
From surfactants to the stratum corneum

Abstract

The work presented in this thesis is dedicated to theoretical development, experimental testing and application of polarization transfer solid-state nuclear magnetic resonance (PT ssNMR). PT ssNMR is an analytical tool, which provides detailed information about molecular mobility in model or simple soft matter systems at the low water content regime, enabling the creation of phase diagrams. Soft matter encompasses not only every-day-use materials, such as medical formulations and washing powders, but also a large variety of biological tissue, for example the stratum corneum (SC). It is useful to characterize molecular mobility at varying conditions, because changing temperature or water content affects macroscopic material properties, for instance permeability, flexibility and toughness. Furthermore, PT ssNMR enables recognition and qualitative description of the coexisting solid- and liquid crystalline phases. Such two-phase coexistence regions dominate the phase diagrams at low water contents, especially in systems equilibrated by contact with humid atmosphere, such as washing powder. In the investigation of complex materials, for example SC, the outer layer of the skin, PT ssNMR provides molecular insight into the mobility of different components, protein and lipid in the case of SC, thus helping to understand and explain properties of the skin barrier.

Key words

solid-state NMR, polarization transfer, molecular mobility, soft matter, biological tissue

Classification system and/or index terms (if any)

Supplementary bibliographical information	Language
	English

ISSN and key title	ISBN
	978-91-7422-302-6

Recipient´s notes	Number of pages	Price
	142	
	Security classification	

Distribution by (name and address)

I, the undersigned, being the copyright owner of the abstract of the above-mentioned dissertation, hereby grant to all reference sources permission to publish and disseminate the abstract of the above-mentioned dissertation.

Signature ___*Agnieszka Nowacka*___   Date _____*April 24th, 2012*_____

List of articles

This thesis is a summary of the following papers. They will be referred to by their Roman numbers throughout the text. The articles are included at the end of the thesis.

I   **Polarization transfer solid-state NMR for studying surfactant phase behavior**
Agnieszka Nowacka, Parveen Choudhary Mohr, Jens Norrman, Rachel W. Martin, Daniel Topgaard
Langmuir, **2010**, *26*, 16848-16856

II   **Signal intensities in ^{1}H-^{13}C CP and INEPT MAS NMR of liquid crystals**
Agnieszka Nowacka, Nils Bongartz, O. H. Samuli Ollila, Tommy Nylander, Daniel Topgaard
Manuscript

III   **Small polar molecules like glycerol and urea can preserve the fluidity of lipid bilayers under dry conditions**
Agnieszka Nowacka, Stèphane Douezan, Lars Wadsö, Daniel Topgaard, Emma Sparr
Soft Matter, **2012**, *8*, 1482-1491

IV   **Molecular mobility of the skin barrier by polarization transfer solid-state NMR**
*Sebastian Björklund, *Agnieszka Nowacka, Joke Bouwstra, Emma Sparr, Daniel Topgaard
*authors contributed equally
Manuscript

List of contributions

I   I performed the experiments and the data analysis. I took part in writing the article.

II   I supervised the experiments. I took part in analyzing the data and writing the manuscript.

III   I supervised the NMR experiments, analyzed them and wrote the NMR part of the article.

IV   I designed the study with Sebastian Björklund. I performed the experiments. I analyzed the data, together with SB, and helped with the writing of the manuscript.

Not included in the thesis:

Filter-exchange PGSE NMR determination of cell membrane permeability
Ingrid Åslund, Agnieszka Nowacka, Markus Nilsson, Daniel Topgaard
Journal of Magnetic Resonance, **2009**, *200*, 291-295

Preface

The work presented in this thesis is dedicated to formulation, development, testing and application of a nuclear magnetic resonance (NMR) based tool for investigating molecular mobility at low water contents. The tool, polarization transfer solid-state nuclear magnetic resonance (PT ssNMR), is a combination of three experiments: direct polarization (DP) for unenhanced ^{13}C spectrum, cross polarization (CP) for enhanced ^{13}C spectrum of the rigid molecular segments and insensitive nuclei enhanced by polarization transfer (INEPT) for enhanced ^{13}C spectrum of the mobile molecular segments.

Acquiring those three spectra for a sample and comparing the signal intensities gives enough information to construct phase diagrams, at low water content, for model or simple systems. For biological tissue, PT ssNMR provides information allowing description of molecular behavior of various components with changing conditions.

In the following summary, I describe the method and results, which can be found in the scientific articles appended at the end of the summary. Articles I and II provide theoretical description of the method, as well as its validation on model systems, while Articles III and IV focus on the application of PT ssNMR.

Agnieszka Nowacka

Lund, 2012

"I almost wish I hadn't gone down that rabbit-hole

- and yet - and yet - it's rather curious, you know, this sort of life!"

Alice, *Alice's Adventures in Wonderland* by Lewis Carroll

Table of contents

Popular scientific summary

The word "motion" usually brings to mind movement from point A to point B. In the world of chemistry, this kind of motion is typically referred to as translational motion. Its consequences are experienced by us every time we smell a scent in the air or watch a dye spread in water. The fragrance is nothing else than molecules that fly in the air. Color is molecules swimming in the water.

In solid materials, translational motion of molecules is hindered or impossible, but it is wrong to think that the molecules do not move at all. In fact, in many materials that appear solid to the eye, molecules fidget quite a lot. Such kind of motion affects the properties of those materials, for example: if we try to bend a plastic spoon, it will break. However, if we put a plastic spoon into a glass of hot water and try to bend it there, it will actually bend. What happened? The polymer molecules, from which the spoon is made, move about more if they are hot, taking away the brittleness of the spoon and making it supple.

The plastic spoon is an example of what we call "soft matter". Another example of soft matter is the outer layer of human skin, stratum corneum. In normal conditions, the molecules making up stratum corneum are quite rigid, acting as a barrier to both, water trying to get out of the body, as well as something from the outside getting in. However, in very humid conditions the molecules in the skin will wriggle and more water, or things from the outside, will be able to go through. When medication has to be applied through skin, increasing humidity is often used to enhance the efficacy of the therapy.

In the case of the spoon it was temperature that changed the properties of the material, while in the case of skin – the amount of water. When designing new soft matter materials, such as the spoon, or understanding their properties, water content and temperature are the most important external conditions. It is so, because those two change on daily basis and a successful material usually has ideal properties: we want a rigid plastic spoon, but a rather flexible car tire. Those properties have to stay the same on a rainy night when the temperature is lower and the humidity of the air considerably high, as well as during a sunny afternoon, or in an air-conditioned room, where the humidity of the air can be very low.

When talking about biological material, also largely encompassed within the soft matter, it is not so much the question of "designing", but more of "understanding". Knowing how much the molecules fidget or what makes them stop is very helpful when trying to understand what makes the living organisms tick. In the long run, this knowledge can lead to designing therapies for diseases, such as Alzheimer's or Parkinson's.

Nuclear magnetic resonance (NMR) is an experimental method, that can be used to measure molecular mobility and predict or explain material properties at different temperatures and water contents. As the name suggests, we work with

nuclei, which are the cores of atoms, that are put into a magnetic field and we can measure their resonance frequencies at that field.

Not all nuclei react to magnetic fields, but those that do can be manipulated to provide information about their state. This information, depending on the exact NMR experiment, can include not only the description of the molecular fidgeting, but also the translational motion and molecular structure, making NMR a versatile and powerful tool. The advantage of NMR is that no modification of the investigated material is required, because the molecules that make up the material we want to measure are composed of atoms that we can use as our informants. Also, NMR is non-invasive, which means that the magnetic field does not change the investigated substance and no destruction of the material occurs during the experiment.

In this thesis, molecular wriggling is described in the terms of rate and directional preference by using two experiments that act as mobility filters. Conducting one experiment leads to response only from the nuclei in the mobile parts of molecules, while the other provides information on the nuclei which reside in the rigid parts of molecules. Obtaining the spectrum from only one of them, or comparing the intensities when both experiments produce a spectrum, presents insight into the degree of fidgeting.
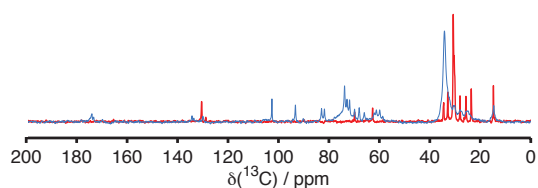
Spectra of dark chocolate. Red spectrum shows signals
from nuclei in wriggly molecules, blue – in the rigid ones.

Introduction

In nature, in the universe, everything moves. The discovery of planetary motion, of the motion of our very galaxy and the galaxies around ours shapes the physics of the modern times. Moving (ideally forward) is the goal of humanity since the times long forgotten.

What about atoms and molecules? Gas particles dash around incessantly and the transport of smell, be it nice or nasty, in air is an easy verification of that fact. Particles in liquids also move, albeit slower than their gaseous counterparts. The diffusion of paint in water can be followed in a glass of water, as well as the flow of the color down the drain, after the painting is done.

And the motion in solid state? Melting sugar crystals into caramel is a consequence of increasing the mobility (the degree of motion) of sucrose molecules. But does sucrose move in the sugar crystals? Translational motion, which allows flow and diffusion in gas and liquid systems, is heavily hindered in solids. However, rotational motion or conformational changes are possible in many materials that appear solid to the eye. Those materials are generally classed as soft matter.

Examples of such materials, plastics and rubber, are affected by the molecular dynamics of their components. For example a polymer that is the main constituent of plastic or rubber goes from soft and flexible to rigid and brittle upon the disappearance of molecular mobility. Such properties need to be considered when designing and producing objects of everyday use, for example, plastic cups or car tires. The consequences of changing polymer mobility can be observed by pouring hot water into a plastic cup designed for holding cold drinks or bending a plastic spoon in a cup of hot coffee rather than breaking it when it is cold. Similarly, designing winter and summer car tires requires knowledge of the properties of the tire components as a function of temperature.

A biological example of a soft matter system is the outer layer of mammalian skin, stratum corneum. The molecular mobility, or the lack of it, of molecules inside this layer limits the transport of water and other substances in and out of the mammalian body, directly affecting its life and health. Also cellular membranes are structures where molecular mobility affects the membrane properties thus affecting the membrane functions and, consequently, the functioning of cells.

The ability to study the mobility of biological systems on molecular scale will lead to deeper understanding of their functioning, while for synthetic materials, it will allow more careful design and less costly trial-and-error in the development of new materials or material applications.

In this thesis, I shall present a nuclear magnetic resonance (NMR) based tool for studying mobility on molecular scale in both simple and complex soft matter systems at low water content.

Why bother with polarization transfer?

As this thesis mainly deals with an experimental technique called nuclear magnetic resonance (NMR), please follow me on a short trip to recap the basics of the method I have used. My aim is to provide a simple explanation for those who are not acquainted with NMR and an elaborate discussion for those who are or are willing to become.

As we go, I will attempt to explain why polarization transfer is useful and what it is exactly. In the second part, I will describe the results that can be expected from using polarization transfer on soft matter materials.

An introduction to NMR

One of the first ^{1}H NMR spectra was recorded in 1951 [Arnold; 1951] and showed three bumps corresponding to the ^{1}H nuclei in three segments of ethanol: CH_3-CH_2-OH, however, the NMR as we know it started with the invention of Fourier transform NMR in 1966, by Richard R. Ernst.

Over the years, NMR grew to be known as a powerful, versatile and, which is possibly the most important in many cases, non-invasive method for studying translational motion (diffusometry), molecular mobility (relaxometry) and even for providing insight into the human body, in the form of clinical magnetic resonance imaging (MRI). It finds application in areas ranging from basic research, through material science, to biomedical problems. It is such a powerful tool, because all we need to perform NMR and MRI experiments is already in the sample we want to measure, excluding the magnetic field that is anyway referred to as "external".

How is that possible? All matter is made of molecules, which in turn are build out of atoms. Each atom is composed of a nucleus and an electron cloud. Each nucleus has an intrinsic property called the spin. The spin of a nucleus can be equal to 0 and then the nucleus does not contribute to the NMR signal, but the spin can also be 1/2, 1, 3/2, 2 and so on. The nuclei with non-zero spin are NMR-active.

What nuclei are those? Nearly every element of the periodic table has at least one isotope that is NMR-active, i. e. has a non-zero spin. This means that matter can be studied without any modifications. Organic matter is rich in ^{1}H, which is by far the most popular NMR spy, but it has also nuclei such as ^{13}C, ^{31}P, ^{14}N and ^{15}N. Inorganic materials are composed of a wider variety of elements, for example ^{29}Si for silica materials or ^{11}B in the case of glass, that can easily be studied as well. Furthermore, magnetic field does not perturb the matter (unless it is magnetic), which is an advantage over the methods that either require labelling (with fluorescent molecules for example) or destroy the sample.

How does NMR work? Using the external magnetic field and radio frequency (rf) pulses, we are able to get signals from our little spies (^{1}H, ^{13}C, …). This signal is highly influenced by the nearest neighborhood of each spy, thus providing us with information about it. With the ability to resolve signals from different spies (like in the case of ethanol spectrum from 1951 – telling apart the ^{1}H signal from CH_3, CH_2 and OH), structural information becomes accessible and by observing the properties of the spies (such as relaxation), dynamics can be deduced.
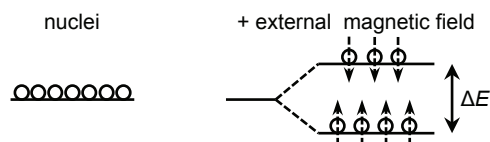

Figure 1 Equilibrium state of NMR-active nuclei ithout (left) and with (right) external magnetic field.

In the work presented in this thesis I only worked with spin-1/2 nuclei, ^{1}H and ^{13}C, so I will focus on them. In a simplified, but very useful description, if an ensemble of atoms with a spin-1/2 is introduced into a magnetic field the nuclei split into two populations, aligned with or against the external field (Fig. 1, Eq. 1), with the energy difference of ΔE (Eq. 2) between them [Hore; 1995]:

$$\frac{N^-}{N^+} = e^{\frac{-\Delta E}{kT}} \, ,\tag{1}$$

where N^- and N^+ are the populations at lower and higher energy with an energy difference, ΔE, at a defined temperature, T, with the Boltzmann constant, k, as the scaling factor. Population difference depends on the energy difference, which can be defined as:

$$\Delta E = h\gamma B_0 \, ,\tag{2}$$

where h is Plank's constant, γ is the gyromagnetic ratio and B_0 is the external magnetic field. The population difference is very small, for example, at the temperature of 300 K, in a 9.4 T external field the N^-/N^+ is $3.2*10^{-5}$ [Hore; 1995]. The NMR signal comes from the difference between the populations, which means that we effectively observe about one in every 10^4-10^6 NMR-active nuclei [Hore; 1995]. Hence, both high gyromagnetic ratio and large amount of NMR-active nuclei in the sample are desirable. The need for high magnetic fields becomes apparent as well, as the higher the field the larger the population difference.

As mentioned previously, ^{1}H is probably the most popular nuclei used in NMR. It is due to its high gyromagnetic ratio ($\gamma = 42.576$ MHz/T), which ensures a large population difference and the high natural abundance of ^{1}H isotope (more than 99.9%) which is a definite plus.

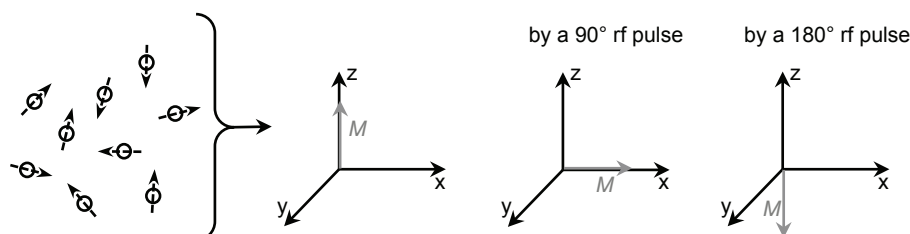Random orientations give net magnetization, *M*, which can be flipped:

Figure 2 Nearly randomly oriented nuclear spins in the external magnetic field (left) create net magnetization, *M*, along the direction of the B_0 field, the z-axis (middle left). *M* can be flipped by rf pulses by an arbitrary angle. Here showing the results of a 90° (middle right) and 180° (right) flip angles.

A more accurate picture of spins in magnetic field, presented in Fig. 2, says that, in equilibrium, the spins are nearly randomly oriented, with a small preference for aligning with the magnetic field, thus creating a net magnetization, *M*, in the z direction [Levitt; 2008], which, by convention, is the direction of the B_0 field.

With the help of radio-frequency (rf) pulses the net magnetization can be flipped around a chosen axis by a defined number of degrees. 90° and 180° pulses are by far most popular in NMR, flipping *M* into the XY-plane or inverting it, respectively, as visualized in Fig. 2. The return to equilibrium is known in the NMR world as T_1 relaxation, often referred to as spin-lattice or longitudal relaxation. The origin of T_1 lies in tiny, local fluctuations of the magnetic field [Levitt; 2008] and its length dictates the minimum waiting time between two repetitions of a NMR experiment.

Furthermore, the spins are not static in the magnetic field (Fig. 3). As soon as a spin is not perfectly aligned along the z-axis, a precession about the direction of magnetic field takes place [Levitt; 2008]. The frequency of this precession is defined by the gyromagnetic ratio of a nucleus and the strength of the external magnetic field, and is called the Larmor frequency, ω_0:
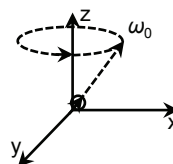
Figure 3 Spin precession about the B_0 field at Larmor frequency, ω_0.

$$\omega_0 = -\gamma B_0 .\qquad(3)$$

A result of a pulse sequence, i. e. a series of rf pulses that make up a NMR experiment, is an oscillating signal in resonance with the frequency of the applied rf pulses (Fig. 4) and is caused by the spins precessing in the XY-plane with the Larmor frequency. This signal is
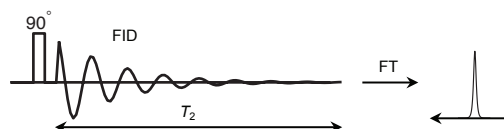
Figure 4 A simple "pulse and acquire" NMR experiment with a resulting FID (left), which can be subsequently Fourier-transformed into a peak (right).

7

called a free induction decay (FID). As the name suggests it decays and its decay is due to the so called spin-spin relaxation (T_2, transverse relaxation). T_2 relaxation is also, like T_1, due to field fluctuations and leads to the spins going out of phase in the XY-plane.

The FID is then Fourier-transformed into a frequency domain form of a spectrum (Fig. 4). Had there been no relaxation, the infinite signal would give rise to infinitely sharp peaks at the resonance frequencies of the measured nuclei. In consequence of the relaxation, the peaks have a finite width and measuring it at the half of the peak height will provide an inverse of apparent, due to B_0 field inhomogeneities, T_2. Because T_2 is influenced by the mobility of the molecule, such a measurement presents insight into the dynamics in the investigated system.

Structural information about the molecules in the sample can be deduced with the help of positions and lineshapes of the peaks, which are a result of interactions with the nearest neighbors of a nucleus. To make a real-life comparison: if you talk to somebody and they repeat a point of view you heard from another person, you know that the speaker has also talked with that person.

In a similar way the effective magnetic field, experienced by a nucleus, depends on the nearest neighbors that are affecting it. This is due to the electrons circling around the nucleus, creating a small magnetic field that adds or subtracts from the external magnetic field, resulting in the field experienced by the nucleus (B) being different than the B_0 by σ – the shielding constant [Hore; 1995]:

$$B = B_0(1-\sigma) \,. \tag{4}$$

Changing the local magnetic field results in slight changes of the Larmor frequency of the spin. Consequently, the oscillations recorded in the FID differ by a small fraction. In liquid state, molecular motion and random tumbling bring the effective influence, which we are able to monitor, down to the neighboring nuclei from the same molecule as the nucleus we are observing. This is the origin of the isotropic chemical shift (δ), which is usually expressed in parts per million (ppm):

$$\delta = \frac{(\nu - \nu_{ref})}{\nu_{ref}} 10^6 \,, \tag{5}$$

where the chemical shift is the difference between the frequency of the measured nucleus (ν) and a reference frequency (ν_{ref}). By convention, the ppm scale (Fig. 5) increases from right to left.

Isotropic chemical shift carries information about the nearest neighborhood of the nucleus: a proton, as ^{1}H isotope is commonly called in NMR, attached to a carbon will have a different chemical shift than a proton bound to an oxygen atom. Further information about molecular structure is given by the scalar couplings, which result in splitting of peaks and are discussed in more detail in the next subchapter (*Solid state NMR methodology*).
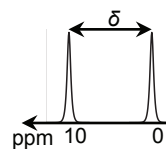

Figure 5 A spectrum of two peaks with the chemical shifts differing by δ.

I have said that ^{1}H NMR is by far the most popular, however, it is not always the optimal choice. There are many protons in nearly all organic compounds and 99% of them will contribute to the NMR signal, creating quite a mess on a small range of chemical shifts (0 to 15 ppm for the most usual molecules), resulting in a rather crowded spectrum. Additionally, the abundance of ^{1}H nuclei leads to many interactions between them, further complicating the analysis of a spectrum. Hence, the scientists often turn to ^{13}C which is also present in abundance in all organic compounds. There are, however, problems that arise when changing from ^{1}H to ^{13}C, such as the low natural abundance (1.1%) of the ^{13}C isotope. The most abundant carbon isotope, ^{12}C, has spin equal to zero and is thus of no use in NMR. In consequence, only about 1% of the carbon nuclei in any molecule is NMR-active, resulting in much lower signal-to-noise ratio in the spectrum. On the other hand, we are rewarded by almost 300 ppm range of isotropic chemical shift values.

A solution to the problem of low abundance, simple in idea, though not always in implementation, is ^{13}C labelling of the molecules. Synthesizing the molecules using only ^{13}C as building material will result in higher abundance. However, even at 100% [13]C signal will be smaller than that of 100% [1]H, because of the difference in the gyromagnetic ratios. For [13]C $\gamma = 10.705$ MHz/T, which is four times lower than that of ^{1}H, resulting in the energy difference between the spin up and down states (Eq. 2), and consequently the population difference of the spin states (Eq. 1), being smaller. A solution to that problem is a technique called polarization transfer and I will describe it in details in further parts of this chapter (*Polarization transfer as signal enhancement technique*).

Solid state NMR methodology

From the descriptions in the previous section, one could think that NMR is fairly straightforward: put a sample into a magnet and record a spectrum. Indeed such is the case if the sample of interest is an isotropic liquid, where random tumbling motion – translational diffusion of molecules combined with rotational motions – leads to averaging of various interactions and consequently, to a simple spectrum.

While the general principle remains the same, studying samples in solid state or even anisotropic liquids, brings out some problems due to the non-averaged

interactions [Laws; 2002]. We no longer have a dilute system, where one molecule barely notices the others and where they all motionally average out to the same result. Now they are crowded in a crystal structure or an amphiphile self assembly and looking at the spectrum is like listening to a crowd: everybody is talking at the same time, but not saying the same or using different words to express themselves. In result, we will probably not realize what the crowd is trying to say.

In NMR the result of listening to a crowd of molecules is a broadened, sometimes to the point of disappearing, spectrum. Two separate phenomena add up to create this effect: couplings between pairs of nuclei and chemical shift anisotropy (CSA). Let us look at the origins of those, starting with the former.

The couplings between nuclei can be divided in two ways: firstly into scalar and dipolar couplings, secondly into homo- and heteronuclear couplings. In the first division the nature of the coupling is different and in the second – the participating nuclei. How do the couplings work? Let us go back to the crowd metaphor and imagine being inside the crowd. Standing next to a person it is very easy to hear what they say and change our own opinion somewhat. Similarly, in the crowded sample, a nucleus feels the influence of other nuclei close to it, which changes slightly its resonance frequency.

As mentioned previously, there are two kinds of couplings, differing with the nature of the coupling (Fig. 6). The scalar couplings stretch through a couple of bonds, becoming weaker with distance. The C-H coupling is usually of the order of 125 Hz, but a C-C coupling is only approximately 33 Hz. In high resolution liquid spectrum, the scalar couplings lead to splittings of the peaks into multiplets (Fig. 6) that can give information about the molecular structure. However, the linewidth in ^{1}H solid-state NMR (ssNMR) is usually too large to observe the splittings. In the case of ^{13}C NMR, where almost every ^{13}C signal is split by couplings with at least one ^{1}H, the resulting multiplets quickly become too complex to analyze.

Dipolar couplings, mediated through-space rather than through the bonds, are much stronger – typically of the order of a couple of tens of kHz between neighboring nuclei in oriented samples. However, the couplings die off as a function of $1/r^3$, where r is the distance between the interacting nuclei. Their exact strength depends on the orientation of the coupling in relation to the external magnetic field and, in isotropic liquids, dipolar couplings average out due to random tumbling of the molecules, as well as fast reorientation of the molecular segments. Once the tumbling motion and

Figure 6 Influence of the scalar (top) and dipolar (bottom) couplings on the spectrum.

the segment reorientation are restricted, the non-averaged dipolar couplings will result in broadening of the signal (Fig. 6).

Both scalar and dipolar couplings occur between two nuclei of the same kind (^{1}H-^{1}H or ^{13}C-^{13}C), as well as two different nuclei (^{1}H-^{13}C). In NMR the influence of the like and the unlike nuclei is not easily separated from the level of the spectrum, but can be selectively eliminated by homo- or heteronuclear decoupling, for like and unlike nuclei respectively, during signal acquisition. Heteronuclear decoupling is easy to perform in comparison to homonuclear decoupling. In the case of recording a ^{13}C spectrum of molecules with natural ^{13}C abundance, the problem of homonuclear couplings solves itself – there are simply too few ^{13}C nuclei for the statistically relevant possibility of having them close enough to influence the spectrum.

Different heteronuclear decoupling schemes are available, ranging in efficiency and the level of complicity [Laws; 2002]. In the case of the studies presented in this thesis Two Pulse Phase Modulated (TPPM) ^{1}H heteronuclear decoupling scheme was chosen [Bennett; 1995]. It is a good balance between efficiency, in the case of most of the investigated samples, and easiness in implementing.

The second problem of ssNMR, the chemical shift anisotropy, can be described on the example of the crowd where everybody may be speaking about the same thing, but not saying the same words at the same time. Listening from afar will result in hearing a distorted noise, rather than getting any information about what the crowd wants.
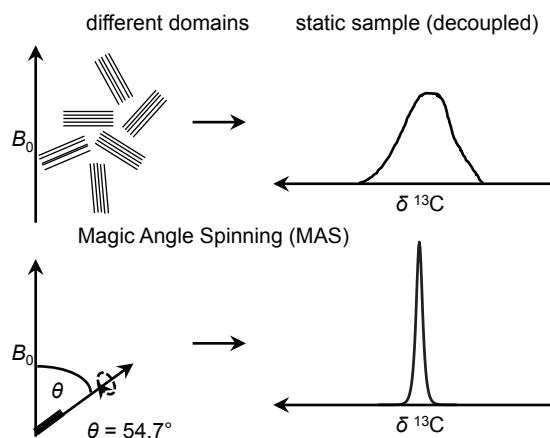
Figure 7 The result of chemical shift anisotropy (top) and the "magic" solution of MAS (bottom) – spinning the entire sample at $\theta = 54.7°$.

In solids and anisotropic liquids this distorted noise comes in a form of signal broadening due to random orientation of molecules. The molecules are ordered in their domains, but unless the sample is a single crystal the domains are random in relation to the external magnetic field (Fig. 7).

It is mentioned in *An introduction to NMR* that the origin of isotropic chemical shift is in the currents induced in the electron cloud surrounding the nucleus. In a molecule the electron cloud is not isotropic and thus the current induced depends on the orientation of the molecule in the external magnetic field. Consequently, the magnetic field induced by the current will depend on the very same orientation and will give raise to different values of chemical shift as the orientation changes. In isotropic liquids the orientation changes so fast that the NMR spectrometer is only able to record their average in the form of a sharp signal at the isotropic chemical

11

shift. In solids and anisotropic liquids the tumbling motion is not possible or hindered and the anisotropy of chemical shift leads to signal broadening.

The chemical shift anisotropy is scaled by the factor of $3\cos^2\theta\text{-}1$, where θ is the angle to the direction of B_0. It so happens that for $\theta = 54.7°$ $\cos^2\theta = 1/3$ and the whole expression becomes zero and thus CSA is cancelled at this particular angle, leaving only the isotropic chemical shift value. Rotating the whole sample about this magical angle has an effect of cancelling the anisotropic term for all nuclei and reducing the spectrum of a solid sample to sharp peaks (Fig. 7), provided that the rate of the rotation is greater than the CSA and the signal is acquired under appropriate decoupling conditions [Laws; 2002]. This technique is called magic angle spinning (MAS).

In the case of spinning at speeds lower than the magnitude of CSA (still assuming decoupling conditions during signal acquisition) the broadened signals of static sample become a multitude of spinning sidebands, spaced out from the isotropic peak at the multiples of the spinning rate [Laws; 2002]. Analysis of the spinning sidebands can give information about the sample as well [Herzfeld; 1980], but it is not in the scope of this thesis.

Polarization transfer as signal enhancement technique

As mentioned in *An introduction to NMR*, ^{13}C NMR poses additional challenges, compared to ^{1}H NMR. Those can be dealt with by increasing the abundance of [13]C (labelling the molecules with ^{13}C) and/or by using techniques for signal enhancement, such as polarization transfer. In those techniques the abundant nuclei, usually protons, are polarized and then the polarization is transferred onto the rare nuclei, in this case [13]C. Both approaches have their advantages and disadvantages. While polarization transfer requires more work for the experimental set-up, acquiring ^{13}C labelled material is expensive and sometimes the choice of research topic includes an implicit choice of the approach to the signal enhancement. For example, getting a hold of ^{13}C labelled, intact stratum corneum is like finding a unicorn: it is much easier to get familiar with polarization transfer.

The two main schemes for polarization transfer are: cross polarization (CP) and insensitive nuclei enhanced by polarization transfer (INEPT). The first, CP, is the most important and basic scheme in solid state NMR [Pines; 1972], while the second, INEPT, is the equivalent for liquid state NMR [Morris; 1979]. INEPT can also be used in ssNMR [Alonso; 2003, Elena; 2005], providing better signal than CP in case of residual molecular mobility (see *The dependence of PT ssNMR on the mobility of molecular segments*).

This thesis presents how CP and INEPT, combined with a simple "pulse and acquire" [13]C experiment (later on referred to as DP, direct polarization) create a new

NMR based tool. This tool, further on referred to as polarization transfer solid-state NMR (PT ssNMR), can be used in the investigation of soft matter.

The idea behind polarization transfer is to use the nuclei with high gyromagnetic ratio (γ) to give the nuclei with low γ a boost [Levitt; 2008]. Going back to our crowd metaphor, we can imagine that there are two kinds of people in the crowd: loud and quiet. In a real crowd we will never hear the quiet ones, but in NMR we have the possibility to listen selectively. The problem remains that the quiet people are, well – quiet. What we would like to do is to have the loud ones somehow teach the quiet ones to be louder, or maybe lend them their voice volume. To be able to do that, the quiet and loud people have to talk together.

That is where polarization transfer comes in the picture, it is like lending a megaphone to rare nuclei, so that they can be better heard. However, for the abundant ^1H to enhance the signal of the rare ^{13}C, the two have to resonate on the same frequency.

To understand that concept let us take a step back and see what happens when we insert ^1H and ^{13}C into a magnetic field. They start to precess at their Larmor frequencies, which depend on the gyromagnetic ratios and the strength of the magnetic field (see Eq. 3, *An introduction to NMR*). The frequency gap between the precession rates is too big for any resonance and nothing can be done to modify it.

Let us imagine that we can induce another magnetic field, such that the angular motion for ^1H and ^{13}C nuclei is the same. Such an angular motion is called nutation and could be understood as the rate at which the net magnetizations of ^1H and ^{13}C nuclei flip from the z axis to the XY-plane to the –z axis to the XY-plane to the z axis and so on. Nutation is induced by rf pulses, simultaneous for ^1H and ^{13}C nuclei and it is possible to adjust the frequency for both because two rf pulses are used – one on ^1H channel (physical connection in the spectrometer, responsible for manipulating ^1H spins and recording ^1H signal) and one on ^{13}C channel. By adjusting the power levels of the rf pulses for ^1H and ^{13}C, we can give them the same nutation frequency (ω_1) and thus make them "talk". This will lead to polarization transfer between the protons and the carbons in the sample, boosting the carbon signal.
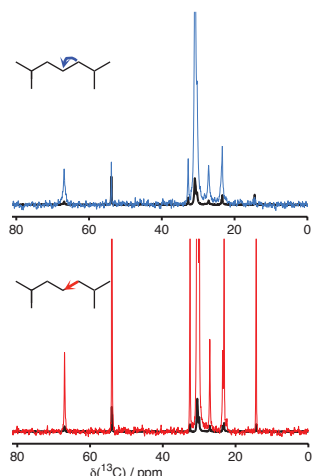
Figure 8 Spectra resulting from a simple carbon experiment (black), compared with CP (blue) and INEPT (red) with the same number of repetitions. The cartoon representations of respective polarization transfer paths are also shown.

The polarization transfer occurs via the heteronuclear couplings between ^{13}C and its nearest ^{1}H nuclei. From the previous section, we know that there are two kinds of couplings possible between nuclei: the scalar and dipolar couplings. The main difference between CP and INEPT is that one uses the dipolar couplings and the other the scalar couplings to transfer the polarization (Fig. 8). In the next section I will discuss how this difference influences the efficiency of both sequences, but for now let us see how they work.

In cross polarization, the 90° pulse on ^{1}H channel is followed by a simultaneous pulse on both channels, during which the nuclei nutate and the polarization transfer takes place (Fig. 9). The power of the ^{1}H pulse is ramped in order to ensure best matching conditions for ^{1}H and ^{13}C nutation frequencies. An obvious factor that influences this transfer is the rate, at which it occurs, R_{CH}, and the duration of the contact time, i. e. the pulse length, τ_{CP}. The pulse length is set by the user, while the R_{CH} depends on the sample, according to [Alemany; 1983]:

$$R_{CH} = \frac{1}{T_{CH}} = \gamma_C^2 b_C^2 j\left(\omega_1^H - \omega_1^C\right), \tag{6}$$

where γ_C is the ^{13}C gyromagnetic ratio, b_C, is the root-mean-square amplitude of the magnetic field fluctuations, resulting from the mobility of the investigated molecules, felt by the carbon nuclei, j is the reduced spectral density and $\omega_1^{H/C}$ are the ^{1}H and ^{13}C nutation frequencies. Spectral density and mean-square amplitude of the field fluctuations will be further discussed in the next subchapter, *The*

Figure 9 CP pulse sequence, where τ_{CP} is the contact time.

dependence of PT ssNMR efficiency on the mobility of molecular segments. The ramping of ω_1^H during τ_{CP} (Fig. 9) can be taken into account by replacing $j(\omega_1^H - \omega_1^C)$ with the following approximation:

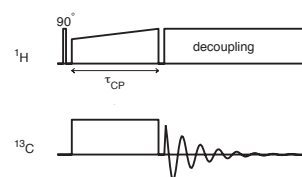$$\overline{j\left(\omega_1^H - \omega_1^C\right)} = \frac{1}{\omega_{1,max}^H - \omega_{1,min}^H} \int_{\omega_{1,min}^H}^{\omega_{1,max}^H} j\left(\omega_1^H - \omega_1^C\right) d\omega_1^H. \tag{7}$$

The final factor influencing the efficiency of CP is the rate of the ^{1}H spin-lattice relaxation in the rotating frame, $R_{1\rho}^H$, setting the time limit during which the ^{1}H nuclei are available for the polarization transfer.

$R_{1\rho}^H$ can be expressed as [Harris; 1986]:

$$R_{1\rho}^H = \frac{1}{T_{1\rho}^H} = \gamma_H^2 b_H^2 \frac{1}{2}\left[j\left(\omega_1^H\right) + j\left(\omega_0^H\right)\right], \tag{8}$$

where ω_0^H is [1]H Larmor frequency and b_H is the root-mean-square amplitude of the magnetic field fluctuations felt by the ^{1}H nuclei.

The signal enhancement obtained with CP, relative to the theoretical maximum signal obtained from a ^{13}C direct polarization (DP) experiment if full longitudal relaxation is allowed between repetitions, can be expressed as [Alemany; 1983]:

$$\frac{I_{CP}}{I_{DP}^{eq}} = \frac{\gamma_H}{\gamma_C} \frac{\exp\left(-R_{1\rho}^H \tau_{CP}\right) - \exp\left(-R_{CH}\tau_{CP}\right)}{1 - R_{1\rho}^H / R_{CH}}, \tag{9}$$

where I_{DP}^{eq} is the theoretical maximum of the ^{13}C signal intensity of the DP experiment, assuming full longitudal relaxation of ^{13}C, and I_{CP} is the experimental intensity of CP signal. The maximum enhancement depends on the ratio of the gyromagnetic ratios of the nuclei participating in the polarization transfer.

The value of contact time, τ_{CP}, chosen in the experiment is a compromise between the R_{CH} and $R_{1\rho}^H$ – it has to be long enough for the transfer to occur, but short enough for the relaxation not to erase the effort (Fig. 10). The final factor to be taken into account is not relevant if merely a ^{13}C spectrum is desired. However, in this thesis the mobility of the molecules is investigated and it is wise to set τ_{CP} to such a value that polarization transfer on to distances larger than one bond length is negligible. In practice it means as short as possible, while still observing efficient CP and in all the experiments τ_{CP} was set to 1 ms.
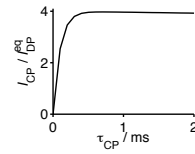

Figure 10 The efficiency of I_{CP}/I_{DP}^{eq} as a function of τ_{CP} length.
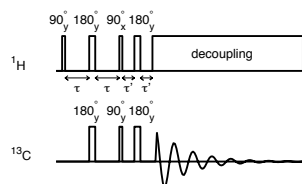
Figure 11 INEPT pulse sequence with τ and τ' evolution times.

In the case of INEPT induced polarization transfer, the ^{1}H excitation pulse is followed by a series of 180° and 90° pulses, simultaneous on both channels (Fig. 11). The role of those pulses is to align ^{1}H and ^{13}C magnetizations and the polarization transfer occurs via the evolution of the scalar couplings, in the waiting times τ and τ'. In this case, the efficiency of the signal enhancement depends on the ^{1}H and ^{13}C spin-spin relaxation rates, R_2^H and R_2^C, limiting the time during which the nuclei are "focused" on their task of transferring the polarization. R_2^H and R_2^C can be expressed as [Harris; 1986]:

$$R_2^{H/C} = \frac{1}{T_2^{H/C}} = \gamma_{H/C}^2 b_{H/C}^2 \frac{1}{2}\left[j(0) + j\left(\omega_0^{H/C}\right)\right]. \tag{10}$$

INEPT induced signal enhancement will also depend on the gyromagnetic ratios of the involved nuclei (^{1}H and ^{13}C in the work presented in this thesis), the strength of the scalar coupling between them, J_{CH}, and the multiplicity of the bond ($n = 2$ for CH_2 group). It can be expressed as [Elena; 2005]:

$$\frac{I_{INEPT}}{I_{DP}^{eq}} = \frac{\gamma_H}{\gamma_C} n \sin(2\pi J_{CH}\tau)\sin(2\pi J_{CH}\tau')\cos^{n-1}(2\pi J_{CH}\tau') \\ \exp\left(-2\tau R_2^H - 2\tau' R_2^C\right) \tag{11}$$

Due to the dependence of INEPT enhancement on the multiplicity of the bond, a compromise must be made between enhancing signals and seeing signals from all molecular segments [Elena; 2005], as shown in Fig. 12. This is done by adjusting the delay times, τ and τ' in the pulse sequence. In the experiments presented in this thesis, τ and τ' were set to 1.8 and 1.2 ms,

Figure 12 The efficiency of INEPT for different molecular segments as a function of τ'.

respectively. Changing τ' can lead to enhancing CH signals or inverting CH_2 signals, which is useful for peak assignment in complicated systems (Article IV).

Figure 13 DP pulse sequence.
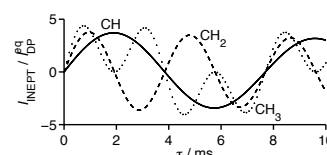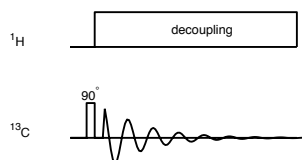
Finally, the last experiment making up PT ssNMR is a direct polarization sequence – a simple 90° pulse on ^{13}C channel, followed by acquisition. The intensity of DP depends on the ^{13}C longitudinal relaxation rate [Harris; 1986]:

16

$$R_1^C = \frac{1}{T_1^C} = \gamma_C^2 b_C^2 j\left(\omega_0^C\right) \tag{12}$$

and on the delay time between the scans t_R. The efficiency of this pulse sequence can be expressed as:

$$\frac{I_{DP}}{I_{DP}^{eq}} = 1 - \exp\left(-R_1^C t_R\right), \tag{13}$$

where I_{DP} is the actual intensity obtained with a finite t_R.

Polarization transfer from ^{1}H to ^{13}C can give the theoretical maximum enhancement of four times ($I_{CP/INEPT} = 4 * I_{DP}^{eq}$), because the gyromagnetic ratio of protons is four times that of carbons. In practice, the enhancement is affected by the behavior of molecules in the sample, which affects the relaxation rates involved, as will be described in the following subchapter.

The dependence of PT ssNMR efficiency on the mobility of molecular segments

The previous section introduced the experiments that make up PT ssNMR and the variables that govern their efficiency. Now time has come to see how those variables, i. e. the relaxation rates, depend on molecular mobility, as it is essential to understand why combining CP and INEPT experiments is of any use. I shall, however, start by a short explanation without equations and variables.

As mentioned previously, CP and INEPT boost the ^{13}C signal through different heteronuclear couplings. This difference has a simple consequence that their efficiency will differ depending on the mobility of molecules in the investigated system. How? Let us have a look back to the scalar and dipolar couplings, because those are the means that INEPT and CP, respectively, use to transfer the polarization from ^{1}H to ^{13}C. In the case of fast reorientation motion or random tumbling of the molecule, the dipolar couplings will get averaged, cutting off the boosting of pathway CP. INEPT, on the other hand, uses the through-bond couplings which stay intact in mobile molecules, thus allowing the polarization transfer and boosting of the signal. In rigid molecules, the

Figure 14 Dependence of signal enhancement on molecular mobility.

scalar couplings are also present, however, in solids, T_2 is so fast that the signal dies before we get the chance to acquire it. Consequently, slow or no molecular mobility will result in efficient CP but no INEPT, while the opposite will be true for fast
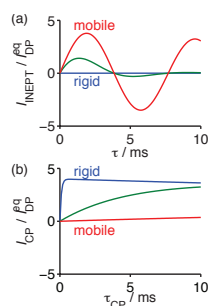
molecular mobility (Fig. 14). The remainder of this chapter is dedicated into a more mathematical description of the phenomena described in this paragraph.

Due to the resolution of obtained spectra (see any of the appended articles or the next chapter), I can talk about the mobility of molecular segments, where by segments I refer to the CH_3, CH_2 and CH groups. To ensure that the polarization stays within the group, the CP contact time is set up to be short enough to avoid transfer to longer distances. In the case of INEPT, the probability of two ^{13}C nuclei next to each other is small enough for the effect to be negligible. In this case the mobility that is influencing the signal intensity the most is that of the C-H bond of the molecular segment. This motion can be described by a two-step model [Halle; 1981], with the help of three parameters: τ_c, τ_s and S. The first parameter, τ_c, motional correlation time, is a measure of the rate of the C-H bond reorientation in an anisotropic domain, while τ_s, is the time it takes for a molecule to go from one anisotropic domain to another (for example one lamellar sheet to another, oriented at a different angle). Finally, the order parameter, S, is the measure of the anisotropy of the C-H bond reorientation within an anisotropic domain.

In the random fields model [Harris; 1986], which was used here (Articles I and II), molecular mobility is responsible for the fluctuations of the magnetic field. In *An introduction to NMR*, I have mentioned that the exact magnetic field experienced by a nucleus is slightly different than the external magnetic field, B_0, due to the neighboring nuclei and electrons (Eq. 4). The mobility of the neighborhood will induce field fluctuations and so the local fluctuating field can be described as:

$$B(t) = bf(t), \tag{14}$$

where b is the same root-mean-square amplitude of the fluctuations as in the previous section and $f(t)$ is describing the fluctuations in time. The former, b, is constant and defined by the C-H bond length and multiplicity, i. e. it is different for CH, CH_2 and CH_3 (Article II). The field fluctuations in time, $f(t)$, can be described by their memory, i. e. a measure of time it takes before there is no correlation between the current and starting field [Harris; 1986]. In NMR the memory of $f(t)$ is most often expressed as the correlation function $g(\tau)$ [Halle; 1981]:

$$g(\tau) = \exp\left(-\frac{\tau}{\tau_c} - \frac{\tau}{\tau_s}\right). \tag{15}$$

The above equation is the simplest way of expressing correlation function (visualized in Fig. 15a). Dealing with anisotropic systems, requires taking the symmetry constraints of the anisotropic domains, expressed as the order parameter, S, into account when constructing the correlation function. Introducing S into Eq. 15, results in a two step correlation function (visualized in Fig. 15a):

18

$$g(\tau) = \left(1 - S^2\right)\exp\left(-\frac{\tau}{\tau_\mathrm{c}}\right) + S^2 \exp\left(-\frac{\tau}{\tau_\mathrm{s}}\right), \tag{16}$$

where, the first step depends on the motional correlation time within an anisotropic domain, τ_c, and the second step on the correlation time of the escape from the said domain, τ_s. The scaling of the steps with S^2 is due to the fact that in the anisotropic domain the C-H mobility is restricted by the order parameter and full loss of correlation is only possible if the bond (with its molecule) escapes from the domain.
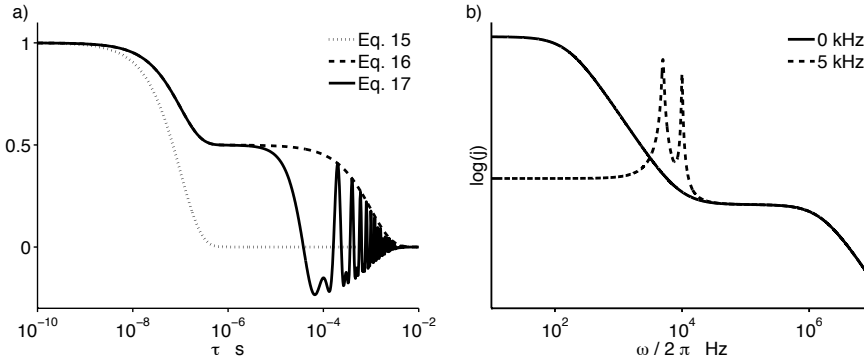
Figure 15 a) Visualization of $g(\tau)$ according to Eq. 15 (dotted line), Eq. 16 (dashed line) and Eq. 17 (solid line). 5 kHz MAS was used for Eq. 17; b) $j(\omega)$ at 0 (solid line) and 5 kHz (dashed line) MAS. τ_c was set to 10^{-7} s, τ_s to 10^{-3} s and S to 0.5.

The influence of MAS (Fig. 15a), with the spinning frequency ω_R, can be introduced to Eq. 16 [Hirschinger; 2006]:

$$g(\tau) = \left[\left(1 - S^2\right)\exp\left(-\frac{\tau}{\tau_\mathrm{c}}\right) + S^2 \exp\left(-\frac{\tau}{\tau_\mathrm{s}}\right)\right]\left[\frac{2}{3}\cos(\omega_\mathrm{R}\tau) + \frac{1}{3}\cos(2\omega_\mathrm{R}\tau)\right]. \tag{17}$$

Fourier transform of Eq. 17 (Article I) gives the reduced spectral density, $j(\omega)$ (Fig. 15b). Thus molecular mobility is introduced into the relaxation times which govern the efficiency of polarization transfer. The best way to continue the discussion is to actually plot the relaxation times as a function of τ_c and see how they change (Fig. 16).

Figure 16 Relaxation times as a function of τ_c. Larmor frequencies were assumed to be 500 and 125 MHz for ^{1}H and ^{13}C, respectively, MAS was set to 5 kHz, $S = 0$ and $\tau_s = 10^{-3}$ s. For th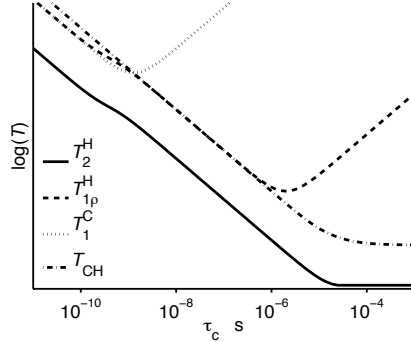e calculation of T_{CH} (Eq. 6,7) $\omega_1^C = 80$ kHz and ω_1^H was ramped from 72 to 80 kHz, $\omega_1^H = 80$ kHz was used for $T_{1\rho}^H$.

The transverse relaxation, T_2^H, as well as the cross polarization time, T_{CH}, decrease monotonously until they reach a plateau, while the other relaxation times, T_1^C and $T_{1\rho}^H$, have a minimum. A consequence of the decrease of T_2^H, is that at some point the magnetization is gone too fast for the INEPT sequence and no signal is obtained (Fig. 17). The shortest longitudal relaxation of carbon nuclei, T_1^C, marks the motional regime where DP is most efficient, i. e. requires the shortest repetition time. Shortening T_{CH} signalizes the increase of polarization transfer efficiency with decreasing τ_c, while the shortest $T_{1\rho}^H$ points out the τ_c regime where the CP experiment fails (Fig. 17). The last phenomena happens to coincide with the so called intermediate motional correlation time regime (Article II).

In the slow and fast motional regime the linewidth is governed mainly by $R_2^{C/H}$, in the intermediate motional regime, i. e. where τ_c is of the order of inverse spinning and rf decoupling frequencies, additional line broadening is induced (Article II):

$$R_{2acq}^C = R_{2d}^C + R_{2\sigma}^C + R_{2res}^C, \tag{18}$$

where R_{2d}^C is the line broadening due to the ^{1}H-^{13}C dipolar interactions, $R_{2\sigma}^C$ is the line broadening that originates from chemical shift anisotropy and R_{2res}^C is the line broadening caused by other, minor mechanisms [Genix; 2006, VanderHart; 1981]. The dipolar term, R_{2d}^C, is given by:

$$R_{2d}^C = \gamma_C^2 b_C^2 \frac{1}{2} j(\omega_{1d}^H), \tag{19}$$

where ω_{1d}^H is the frequency of the ^{1}H decoupling rf pulse. The CSA contribution, $R_{2\sigma}^C$, can be written as:

$$R_{2\sigma}^C = \gamma_C^2 b_\sigma^2 \frac{1}{2} \left[j(0) + j(\omega_0^C) \right], \tag{20}$$

where b_σ is the root-mean-square amplitude of the fluctuating field due to the CSA. It can be expressed by:

20

$$b_\sigma = \frac{B_0 \Delta\sigma}{\sqrt{5}}, \tag{21}$$

where $\Delta\sigma$ is the magnitude of CSA.

The signal broadening induced by the interference of the motional correlation time with MAS and decoupling leads to near disappearance of the DP signal in the very same range of τ_c where CP fails due to fast $T_{1\rho}^H$. Because there is no INEPT in this regime, due to fast T_2 relaxations the result is that of disappearing peaks, as presented in Article II.
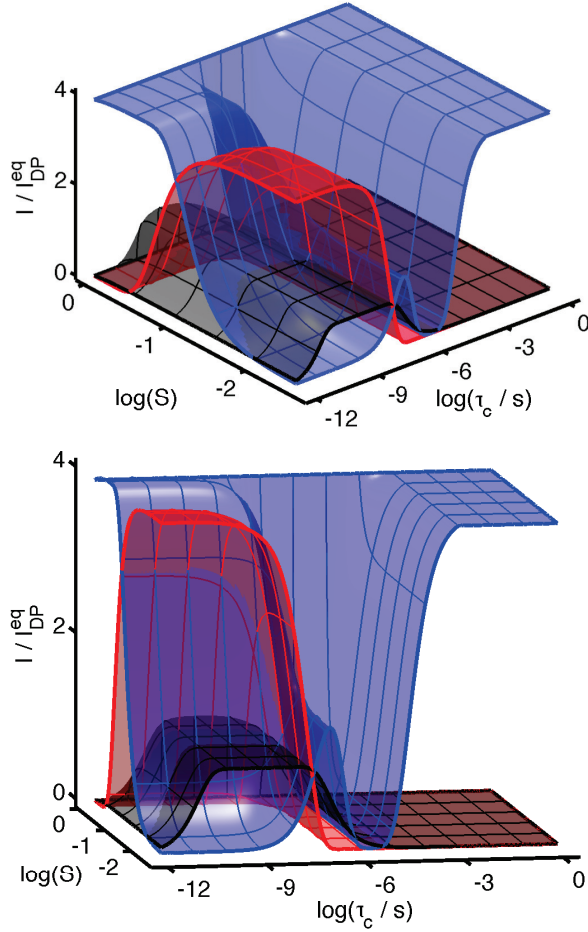

All the dependences on τ_c and S are visualized in Fig. 17, where I_{DP}/I_{DP}^{eq}, I_{CP}/I_{DP}^{eq} and I_{INEPT}/I_{DP}^{eq} are plotted in black, blue and red, respectively, according to Eq. 9 (CP), 11 (INEPT) and 13 (DP).

In the slow motional correlation time regime only CP signal is present, until the motional correlation values of the order of $\tau_c \approx 10$ µs, where the fast $T_{1\rho}^H$, as well as the line broadening effects of MAS and ^{1}H decoupling, lead to signal disappearance. At $\tau_c < 1$ µs I_{CP} reappears and I_{DP} appears. At $\tau_c \approx 0.1$ µs I_{INEPT} joins in and at motional correlation times faster than 1 ns, it is the order parameter that dictates the signal intensity ratios. No I_{CP} can be observed at the order parameter values of $S < 0.05$. I_{CP} increases with increasing S, while I_{INEPT} decreases. At approximately $S \approx 0.1$, $I_{CP}/I_{DP}^{eq} = I_{INEPT}/I_{DP}^{eq}$ and I_{INEPT} continues to decrease until complete disappearance at $S > 0.5$

Figure 17 I_{DP}/I_{DP}^{eq} (black), I_{CP}/I_{DP}^{eq} (blue) and I_{INEPT}/I_{DP}^{eq} (red) as a function of τ_c and S, plotted according to Eq. 9, 11 and 13. Larmor frequencies were assumed to be 500 and 125 MHz for ^{1}H and ^{13}C, respectively, MAS was set to 5 kHz and $\tau_s = 10^{-3}$ s. In CP $\omega_1^C = 80$ kHz and ω_1^H was ramped from 72 to 80 kHz and $\tau_{CP} = 1$ ms. In INEPT $\tau = 1/4*J_{CH}$ and $\tau' = 1/8*J_{CH}$, where $J_{CH} = 130$ Hz. Repetition time $\tau_R = 5$ s was used for DP.

Having bothered, what can we expect as results?

From the previous part, we know that the relative signal intensities of PT ssNMR provide us with information on the mobility of molecular segments. Using PT ssNMR implies that we are interested in systems in dry or nearly dry state, where mobility can change on observable scale as a function of experimental conditions that we are able to implement. This crosses out interest in materials such as glass or porcelain and rather implies that organic and biological materials will be measured. Such materials were mentioned in the introduction and I will now introduce them with some more detail and present the results obtained with PT ssNMR.

Soft matter and NMR

Why is soft matter interesting? For starters, a considerable portion of biological tissue can be classified as soft matter, for example, the lipid systems that include the stratum corneum and cellular membranes. The former is the outer layer of mammalian skin and the barrier protecting the inside of a mammalian body from the outside environment [Forslind; 2004]. Being able to observe the molecular behavior of the components of the stratum corneum, with changing conditions, provides a grasp on how its functions are affected by the changes, of temperature and humidity of the air, that occur on daily basics. A good picture of the molecular details can also help to understand the anomalies that cause skin diseases and find a way to counteract them. The response of other lipid systems, such as the cellular membranes, to changing conditions, increasing osmotic stress for example, affects the functioning of the cells and thus it is also significant in trying to understand the living organisms.

Another example of soft matter in biological tissue are proteins. Their structures, functions and interactions are of fundamental importance, as proteins are necessary for maintaining biological processes in the body. The misfolding of proteins can cause severe problems, for example, it is associated with the Parkinson's disease, where aggregates of fibrillar structure of α-synuclein have been found in the brain cells [Wakabayashi; 2007]. Understanding the mechanisms behind the fibril formation, as well as the interactions of the proteins and their aggregates with their environment, can lead to the understanding of the diseases and, hopefully, the ability to cure or counteract them.

Apart from biological tissue, which is interesting for the very reason that our bodies are made of it, soft matter surrounds us in daily life. Starting from shampoos, creams and washing powders, through yoghurts and chocolate, and finishing with plastic and car tires, we are surrounded by materials entirely or partially composed of polymers and/or surfactants. Understanding their properties with changing conditions is necessary to create stable products: a cream that remains creamy after a

couple of months of shelf life; a winter car tire that does not become too brittle during winter in the north of Sweden; a washing powder that retains the form of dry globules even after hours or days of contact with humid atmosphere.

A large portion of soft matter falls into a sort of gray area of NMR: definitely not liquid, but with considerable molecular mobility, thus not really solid. "Liquid" in NMR is the domain of INEPT [Bussy; 2011] and means solution – samples where CSA and dipolar couplings average out. "Solid", on the other hand, is the domain of CP [Robert; 2001] and MAS, with ceramics and inorganic glass – materials that have the molecular mobility comparable to that of a rock.

The rate of the molecular motion in soft matter materials, even at low water contents, might approach that of the solutes in liquids, but the anisotropy and high density prevent full averaging of the influence of spin-spin couplings and the chemical shift anisotropy. Thus, solid-state NMR is preferable in the investigation of such materials. MAS and heteronuclear decoupling (see *Solid state NMR methodology*) can remove the effects of limited mobility and lead to reasonably high resolution of the spectra while the interplay between INEPT and CP signal intensities provides insight into the molecular mobility. Because investigated systems are usually literally soft (comparing to a rock again), MAS was adjusted not to deform the samples and set to 5 kHz throughout the studies presented below.

The relevant temperature range for biological and synthetic soft matter materials is approximately -5° to 60° Celsius, or 268 to 333 Kelvin, possibly with the exception of the winter car tires in the north of Sweden. Such a range is easily accessible in NMR.

The real-life examples that I have mentioned in previous paragraphs are often in prolonged contact with the atmospheric air (skin, washing powder) and thus their water content is dictated by the equilibration with the relative humidity (RH) of the air. It seems logical to exercise similar equilibration in investigation of the skin or a possible tablet coating material, however, that is not the only reason to choose such an approach. While mixing a predefined amount of water into a sample might, in some cases, be faster and simpler, RH can be easily correlated to water activity (a_w) and osmotic pressure (Π_{osm}), through the relation presented in Eq. 22 [Evans; 1999]. Both a_w and Π_{osm} are of importance in terms of relating the experimental conditions to those occurring in the biological tissue.

$$RT \ln\left(\frac{RH}{100}\right) = RT \ln(a_w) = \Delta\mu_w = -\frac{1}{V_w}\Pi_{osm}, \qquad (22)$$

where R is the gas constant, T is the temperature and V_w is the volume of water.

The absolute water content, expressed in weight percent (wt%), can be subsequently obtained through a gravimetric measurement, ^{1}H NMR signal deconvolution or a sorption microbalance measurement.

24

Amphiphilic molecules as model systems

Every project starts with small steps. In science, those first, small steps are usually in choosing a simple model system and testing a new tool or a hypothesis on it. In the NMR discussion I have presented a new tool, PT ssNMR, together with a model of the expected results. I have also, in the previous subchapter, expressed interest in soft matter systems, such as the stratum corneum, cellular membranes and protein fibrillar aggregates.

It seems like a reasonable next step to choose a model system and test how good PT ssNMR really is. A suitable model of a biological membrane is a membrane composed of one or two kinds of lipids, while the equivalent for washing powder or tablet coating is a surfactant system. Both lipids and surfactants belong to amphiphilic molecules, for reasons discussed below. The systems studied in this thesis, be it simple or complex, synthetic or organic, are mainly composed of amphiphiles and thus the most important properties of this class of molecules are quickly discussed in the remainder of this subchapter. The molecular structures of the surfactants and lipids used as model systems, both in the appended articles and in the following sections, are presented in Fig. 18.

Certain polymers can also be considered amphiphilic, but the work presented in this thesis does not include them and they will be omitted in further discussion.
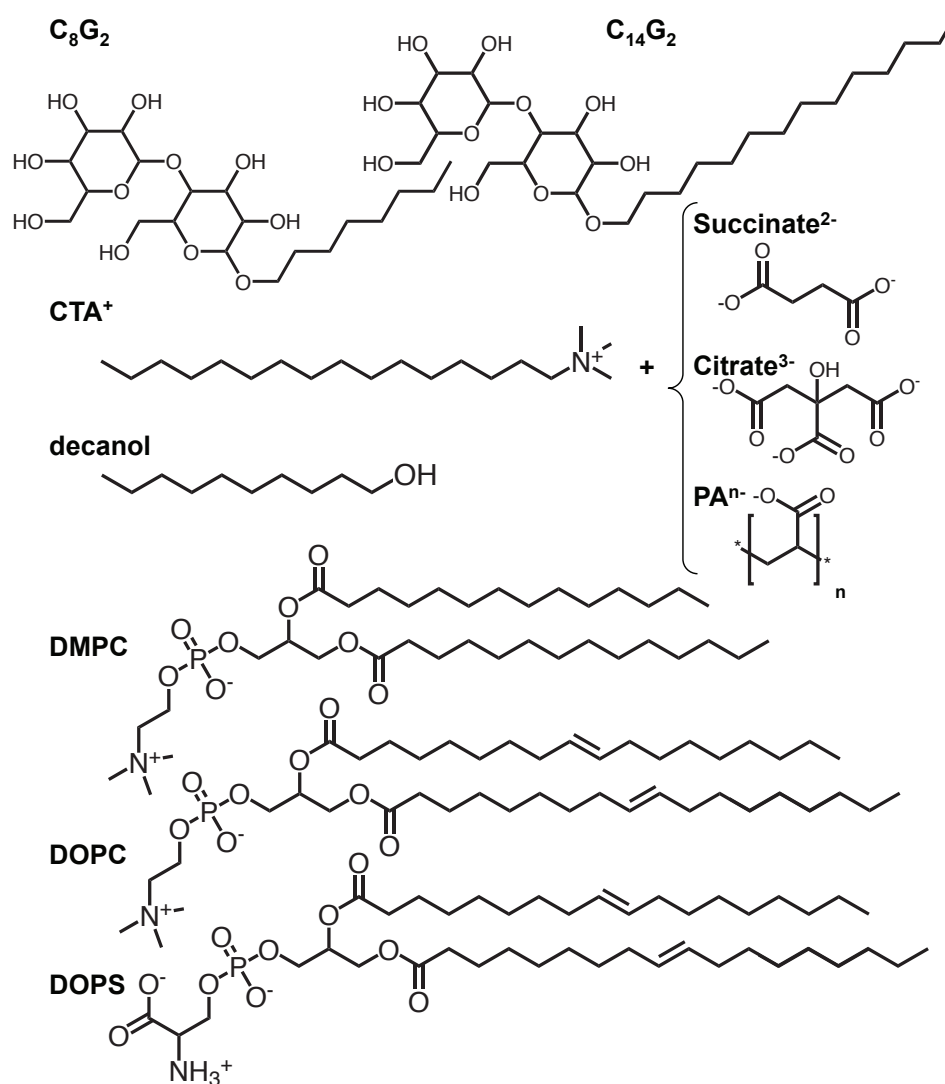
Figure 18 Molecular structures of n-octyl-β-maltoside (C₈G₂), n-tetradecyl-β-maltoside (C₁₄G₂), cetyltrimethylammonium ion (CTA⁺) with the organic counterions used (where PA is polyacrylate), decanol, 1,2-dimyristoyl-*sn*-glycero-3-phosphocholine (DMPC), 1,2-dioleoyl-*sn*-glycero-3-phosphocholine (DOPC) and 1,2-dioleoyl-*sn*-glycero-3-phosphoserine (DOPS).

The property that gives amphiphilic molecules their name is a result of their molecular structures, which can be divided into two parts. The first part is often called a head or a headgroup and it is hydrophilic, which means "water liking". It can contain one (CTA⁺) or more (DMPC) charges and/or function groups with high water affinity (C₁₄G₂).

The other part is hydrophobic / lipophilic, which means "water fearing" / "oil liking", and is usually called a tail or a chain. It is composed of a hydrocarbon chain

(CH_3-$(CH_2)_n$-). Most amphiphilic molecules have either one (CTA^+) or two (DMPC) hydrophobic chains, which may also contain unsaturated bonds (DOPC).

Having both of the above described parts makes surfactants and lipids both lipo- and hydrophilic and thus they are called amphiphilic, which means "liking both".

Once put into an aqueous environment, amphiphiles organize to minimize the possibility of the chains being in contact with water. In doing so, the molecules form the so-called self-assembly structures. The characteristics of this assembly depend on factors such as concentration and molecular structure, but also on the presence of other molecules in the system (Article I). In excess solvent the dominating structures formed by amphiphilic molecules are micelles and vesicles, while at low water content liquid crystalline (LC) self-assembly structures with differing symmetry are formed. Examples of the low water content self-assembly structures are presented in Fig. 19, while a more elaborate discussion can be found elsewhere [Evans; 1999].
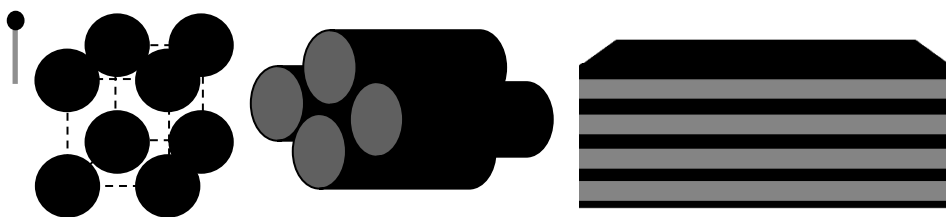

Figure 19 A cartoon of a surfactant with a black headgroup and grey tail (to the left) and the possible liquid crystalline self assembly structures: micellar cubic, hexagonal and lamellar (from left to right).

Validation of PT ssNMR

As I have pointed out in the beginning of the previous subchapter, a new method requires a choice of simple systems on which it can be tested and validated. The systems chosen were CTA^+ with succinate^{2-} as counterion (Article I) and a sugar surfactant, C_8G_2 (Article II). For the molecular structures of both, see Fig. 18 in the previous section.

The results from $(CTA)_2Suc$ and C_8G_2 are presented in Articles I and II, respectively. Here, I will use the results from other model systems, which have also been measured with PT ssNMR, to illustrate what can be seen and concluded from using this method on model soft matter systems.

The first step, of the method validation, was to prepare samples where the surfactant self-assembly structure was known, to see how big are the differences between the relative signal intensities (Article I). The conclusion was: big enough (Fig 20).
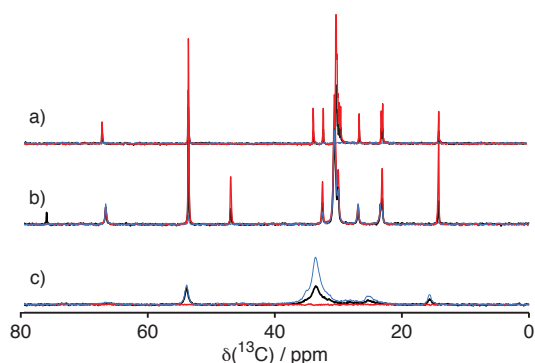
Figure 20 PT ssNMR spectra (DP in black, CP in blue and INEPT in red) of: a) (CTA)₂Suc in LC cubic phase; b) (CTA)₃Cit in LC anisotropic phase; c) (CTA)₃₀PA in solid phase. See Fig. 18 for molecular structures.

Just by looking at the spectra isotropic (cubic) LC, anisotropic (lamellar, hexagonal) LC and solid phases can be told apart. In the cubic phase (Fig. 20a), the signal intensities observed are $0 \approx I_{CP} << I_{DP} < I_{INEPT}$, which is in agreement with fast and isotropic dynamics ($\tau_c < 0.1$ µs and $S < 0.05$). In anisotropic LC (Fig. 20b) each experiment gives raise to a spectrum with similar signal intensities, $I_{CP} \approx I_{DP} \approx I_{INEPT}$, which is possible for a broad range of motional correlation time and order parameter values ($\tau_c < 0.1$ µs and $0.5 > S > 0.05$). For solid phases, where slow dynamics and/or high order parameter ($\tau_c > 10$ µs and/or $S > 0.5$) are expected, INEPT experiment provides no spectrum (Fig. 20c) and the intensity ratios are $I_{CP} > I_{DP} >> I_{INEPT} \approx 0$, providing clear difference from the LC phases.

This itself makes PT ssNMR a worthwhile tool as it bridges the gap between crystalline and locally disordered LC assemblies. Small, gradual changes in relative intensities accompany temperature changes, but first order phase transitions [Atkins; 2006] are marked by jumps of intensities, which can be followed through a more quantitative analysis of a series of spectra.

More information can be gained from a closer study of the individual spectra. In the case of the solid samples (Fig. 20c), no INEPT signal is visible, but the CP spectrum can look considerably different, as shown in Fig. 21. Stretching of the chain, into the so-called all-trans conformation in the crystalline structures, leads to a shift of the isotropic chemical shift values [Earl; 1979], making it possible to tell apart crystalline structures (Fig. 21a and b) from amorphous solids (Fig. 21c), where chains are in random conformation. Furthermore, different crystalline structures provide different CP spectra [Harris; 2006]. In Article I the differences observed are very small, but in Fig. 21a and b they are clear at first glance.
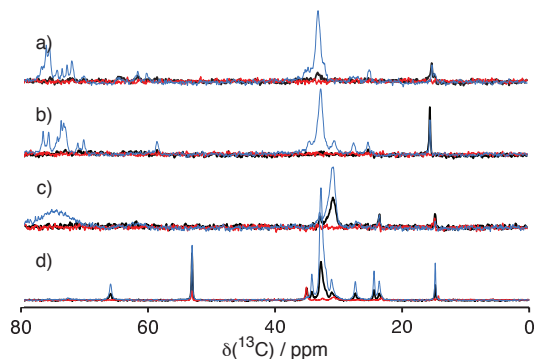

Figure 21 PT ssNMR spectra (DP in black, CP in blue and INEPT in red) of different solid structures of C₁₄G₂ in different crystalline structures (a and b) and an amorphous phase (c); and (CTA)₂Suc in gel phase (d).

28

The gel phase (Fig. 21d) deserves a paragraph on its own. Because the molecules in a gel are stretched, like in the crystalline structures, the CP spectrum resembles that of a crystalline solid (Fig. 21a and b). However, rotational motion of the molecules gives rise to a spectrum with sharp, single peaks, rather than broader or split peaks characteristic for crystals (Article I). The presence of a small, INEPT peak of the succinate[2-] counter-ion (Fig. 21d) points to high mobility in the water layer, which is consistent with freely diffusing water – another important feature of the gel phase.

The possibility to distinguish between gel, amorphous (glassy) and different crystalline phases adds valuable information about the system.

Another consequence of the chemical shift difference between the stretched and random chain conformations is the possibility to detect the presence of coexisting crystalline and LC phases (Fig. 22). This can be done by analyzing the CP spectrum and the presence or the lack of the corresponding INEPT peaks (Fig. 22b). Such phase coexistence is observable even at a very small fraction of one of the phases (Article I).
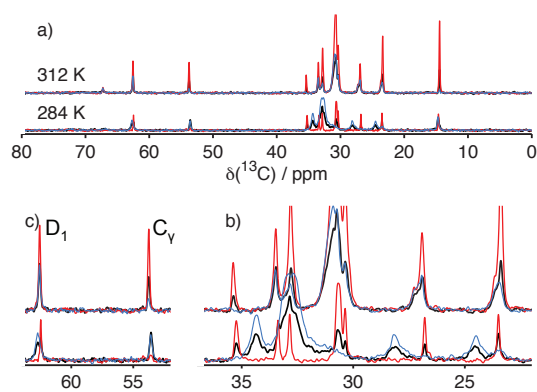

Figure 22 PT ssNMR spectra (DP in black, CP in blue and INEPT in red) of: a) (CTA)₂Suc/decanol/water measured at two temperatures; b) magnification of the CH₂ region of the spectra with visible phase coexistence; c) two peaks that allow qualitative description of the coexisting phases.

In Fig. 22, the PT ssNMR spectra of a mixture of $CTA_2(Suc)$, decanol and water are presented (see Fig. 18 for molecular structures). At 284 K, crystalline phase is clearly visible, due to the presence of the all-trans shifted CP peaks at approximately 24, 28, 33 and 34 ppm (Fig. 22b). Simultaneously, the INEPT peaks of the corresponding molecular segments are visible at some 1-3 ppm less, signalizing the presence of the second phase in the sample, this time liquid crystalline with random chains.

In such a simple system it is even possible to pinpoint a peak characteristic for each component (Fig. 22c), and qualitatively describe the composition of the coexisting phases.

In the case of amorphous solid coexisting with a LC phase broad CP peaks (Fig. 21c) will hint on the phase coexistence.

Phase coexistence of a crystal and an amorphous phase (Fig. 23a) or of two different crystal structures (Fig. 23b) can also be observed but the latter requires previous knowledge about the single structure spectra.

It has to be mentioned that the PT ssNMR spectra are not enough to define the crystalline structure and thus that information was obtained from previous studies on $C_{14}G_2$,

Figure 23 PT ssNMR spectra (DP in black, CP in blue and INEPT in red) of $C_{14}G_2$: a) coexistence of a crystalline and an amorphous phase; b) coexistence of two crystalline phases.

where X-ray powder diffraction measurements were conducted [Ericsson; 2005].

To a smaller scale, INEPT also provides different spectra for different phases, allowing the distinction between bicontinuous and micellar cubic LC phases (Article I).

This impressive collection of information available from PT ssNMR spectra makes it a powerful tool for phase diagrams at low water content regime (Articles I and III), even more can be concluded (Article II).
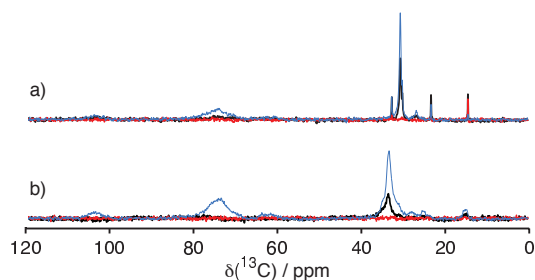

Figure 24 PT ssNMR spectra (DP in black, CP in blue and INEPT in red) of $C_{14}G_2$ ordered lamellar phase at a) 331 K and b) 275 K; illustrating the peak disappearance as a result of phenomena described in Article II.

When I discussed intensity ratios, expected for the different self-assembly structures, in the beginning of this subchapter, I have omitted the regime of $0.1 < \tau_c < 10$ µs. Under the MAS and decoupling conditions chosen in the studies presented in this thesis, it is the regime where the molecular mobility interferes with MAS and decoupling frequencies, resulting in peak broadening [Harris; 1986]. In the same regime, the DP and CP fail due to slow T_1^C and fast $T_{1\rho}^H$, respectively. Because INEPT is no longer present, due to fast T_2, the disappearance of DP and CP results in $I_{CP} = I_{DP} = I_{INEPT} = 0$ (Fig. 24a).

While annoying if we are after a spectrum, this phenomena are quite useful when studying glass transition which, rather than a first order phase transition, is a process of constantly changing mobility. In the case of surfactants we talk about glassy crystals [Kocherbitov; 2004] rather then glass, which is a more polymer concept, but in both cases the structure of the self-assembly does not change, only the molecules slow down their motion. The transition from glassy to liquid crystal
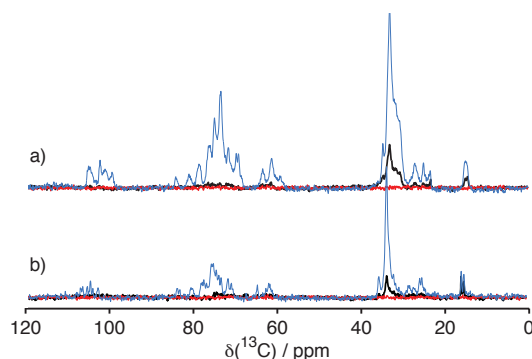
affects macroscopic material properties and thus its characterization is of great interest in material science.

Application of PT ssNMR

Having ensured the usefulness of the tool, natural next step is to apply it to a problem in hope to solve it.

Until now, I have discussed surfactants and their behavior. The naturally occurring counterpart of surfactants are lipids, a class of molecules abundant in biological tissue. They form self assembled structures, alike those of the surfactants, although arguably, lamellar phase is the most common, as lipids make up the membranes in all living cells, as well as the outer layer of the skin, stratum corneum.

Taking a glance at the molecular structures presented in the previous section (Fig. 18), you can notice a couple of molecules that I have not yet mentioned in this thesis. DMPC, DOPC and DOPS are examples of the so called phospholipids, which are major lipid components of various cellular membranes.
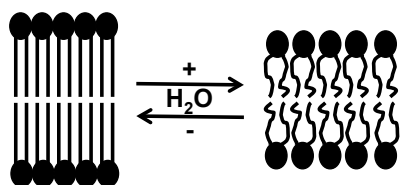

Figure 25 Solid to LC phase transition as a result of changing water content.

A very important feature of a membrane is its ability to go from liquid crystalline to solid phase upon dehydration (Fig. 25), which can occur as a result of drying, but also freezing of a membrane [Ramløv; 2000]. Various organisms have protection mechanisms against dehydration or osmotic stress [Yancey; 1982], which can also act to provoke a phase transition in a membrane [Markova; 2000]. The protection mechanisms are often based on production of small molecules, with low vapor pressure, sometimes referred to as humectants. An example of a humectant is glycerol (Fig. 26), produced by insects that are subjected to low temperatures [Ramløv; 2000]. It also acts as a cryoprotectant in larger organisms [Storey; 1986], such as the Siberian salamander, which can survive several years at -45° C. Human skin has its own protective mixture, called the natural moisturizing factor (NMF), composed of, among others, glycerol, urea and free amino acids [Rawlings; 2004]. An important function of NMF is to keep the skin hydrated and its absence is linked to pathological conditions of extreme skin dryness [Marstein; 1973].

There is a contradiction around the mechanism of this effect, with theories suggesting either direct lipid-humectant interactions [Anchordoguy; 1987] or unspecific binding [Westh; 2003].
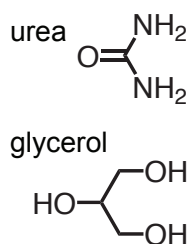
urea

O=C(NH$_2$)NH$_2$

glycerol

HO—CH$_2$CH(OH)CH$_2$—OH

Figure 26 Urea and glycerol.

Studying an intact cellular membrane is very challenging because of the multitude of different molecules and mutual interactions which make it difficult to pinpoint the actual effect that humectants might have. Thus model membranes, composed of one or few different phospholipids are often used as an approximation of the real membrane. They are usually well defined, providing opportunity to investigate the influence of, for example, humectants. In the study described in Article III DMPC was chosen for this role, while the humectants used were glycerol and urea (Fig. 26). The choice of humectants was based on the fact that they are components of NMF and we hoped to later relate the observations of their influence in a simple system to the stratum corneum. Furthermore, glycerol and urea (undercover as "carbamid") are commonly used in cosmetic formulations as moisturizers.

The aim of the DMPC study was to introduce humectant molecules into DMPC bilayers and observe their influence on the lipid phase transition upon dehydration. Pure DMPC undergoes a phase transition from solid to LC at 94% RH, at 27° C [Markova; 2000], thus it is solid at 84% RH, as can be seen in Fig. 27c. In the presence of as little as 1 wt% of glycerol or urea of the dry sample, DMPC bilayers enter a two-phase region at approximately 84% RH at 27° C, as deduced from the sorption microbalance measurements shown in Article III and in previous studies [Costa-Balogh; 2006]. Upon the addition of 10 wt% of urea or glycerol, no solid phase is visible at 84% RH (Fig. 27a and b) at the same temperature. This signalizes that both humectants help preserving LC phase at lower water contents. Both molecules induce a broad two-phase region (Article III). Simultaneously, no specific interaction between glycerol or urea molecules with any segment of the DMPC lipids could be observed in the spectra.

A small drawback of NMR is that it is rather tedious to prepare samples at very many relative humidities or sample compositions, to precisely define the compositions at which phase transitions take place. In Article III, this was remedied with the help of sorption microbalance, where step-wise increase of air humidity and a very accurate balance allow a measurement of water uptake as a function of

Figure 27 PT ssNMR spectra (DP in black, CP in blue and INEPT in red) of: a) DMPC with 10 wt% glycerol at 84% RH; b) DMPC with 10 wt% of urea at 84% RH; c) pure DMPC at 84% RH. Spectra were acquired at 27° C.

relative humidity. The change of water uptake slope accompanies events such as phase transitions.

Combining the information obtained from NMR and sorption measurements made possible a construction of a phase-map, illustrating the influence of

humectants on the lipid bilayers (Article III). The conclusion of the study was that the phase transition occurs at the same solvent content in wt%, regardless of the solvent composition (Article III). Thus the lipids behave as though they were hydrated also under dehydrated conditions if urea or glycerol are present.

The great similarities between the influence of glycerol and urea in terms of water content and solvent composition, as well as the lack of any particular changes in the behavior of DMPC observed in the NMR spectra, point to an unspecific interaction as the mechanism of the moisturizing effect. This suggests that similar results can be expected in other lipid systems.

Taking it up a notch: stratum corneum

While I was describing the abundance of lipids in biological tissue, I mentioned not only the cellular membranes, but also the stratum corneum (SC), the outer layer of the skin. It is the barrier between the inside of the body and the outside, and as such it is subjected to a high water gradient and osmotic stress. Because of its vital importance for mammals, including of course human beings, it is an object of interest and extensive research [Bouwstra; 2001, Jokura; 1995, López; 2007, Rawlings; 2003]. Understanding the details of its structure and the influence caused by the exterior conditions is of great consequence in medical (skin diseases, topical drug therapy) and cosmetic (moisturizers) applications. In the study presented in Article IV the main interest was the influence of hydration and temperature changes on the behavior of the components of SC.

The schematic structure of stratum corneum, as well as examples of molecules that can be found therein, are presented in Fig. 28.
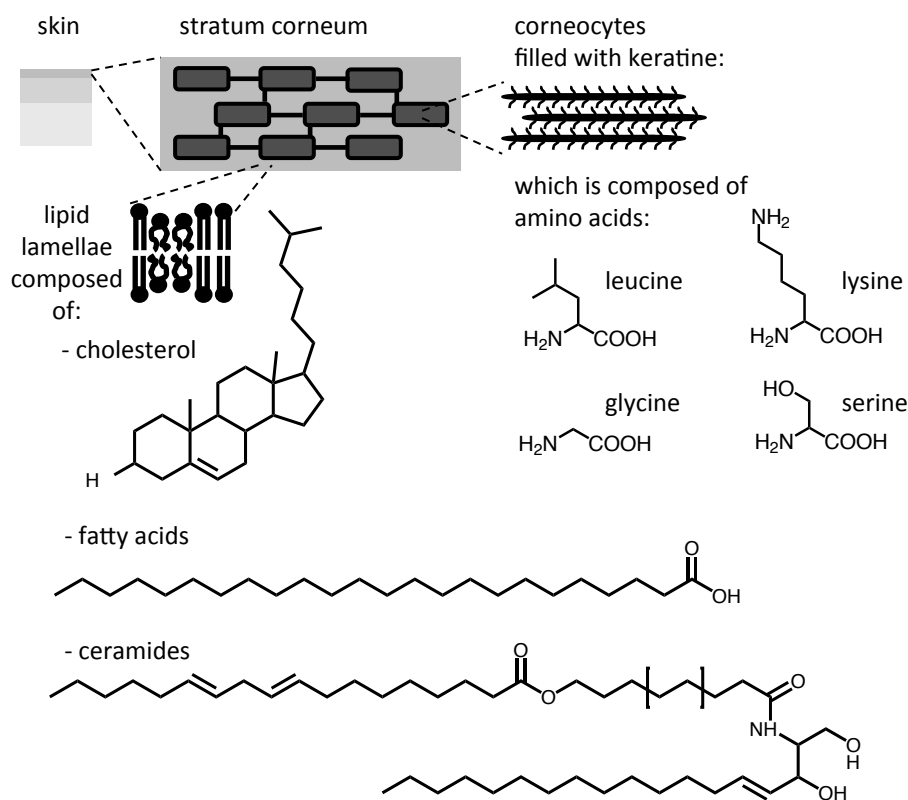
Figure 28 A cartoon of the brick and mortar like structure of stratum corneum, the outer layer of the skin, where bricks are keratine-filled corneocytes connected with corneodesmosomes and mortar is lipid lamellar matrix. Examples of molecular structures of amino acids forming keratine, as well as the lipids found in the lipid lamellar matrix are also shown.

Stratum corneum is a very complicated system not only in the terms of multitudes of different molecules that make it up, but also in the complexity of the self assembly structures that gives it its properties. As can be seen from Fig. 28, it is composed of corneocytes and lipid lamellae. More precisely, it has 10 to 30 layers of corneocytes connected with corneodesmosomes [Forslind; 2004] and embedded in an extracellular, lipid lamellar matrix [Rawlings; 2003]. This structure is often called the brick and mortar model with the bricks being the corneocytes and the mortar – lipid matrix, the only continuous phase of the SC. The lipids are approximately 17 wt% of the dry SC weight, while the rest is protein material [López; 2007].

Corneocytes are dead cells filled with keratin, the structure of which is thought to be stiff rods in a so-called coiled-coil conformation, with disordered side chains [Jokura; 1995]. They are enclosed in a two-layered cornified envelope (CE) [Forslind; 2004]. The innermost layer is made up of various proteins, mainly loricin, which makes up 65-70 wt% of the CE in human SC [López; 2007], and involucrin. The outermost is a layer of fatty acids and ceramides, lipids composed of a fatty acid and a sphingosine part (see Fig. 28), covalently bound to the protein. It has been

34

proposed that the covalently bound lipids act as a matrix for structuring the rest of the lipid material [Rawlings; 2003].

Besides the ceramides and fatty acids, the lipid lamellae are composed of cholesterol and cholesterol esters. While cholesterol has, of course, only one molecular structure, there are eight types of ceramides present in human skin, with different headgroups and chain lengths. The chain lengths are also differing in the case of fatty acids, with the C_{16}-C_{24} long ones being the most abundant. The approximate weight percent composition of the lipid lamellae is detailed in Table 1.

The structure of the lamellae has been a subject to heated discussion, although it is generally agreed that most lipids form a crystalline or gel phase under ambient conditions, which warrants a low permeability, of both hydrophobic and hydrophilic molecules, through the SC [Forslind; 2004]. The most common model predicts approximately 13 nm thick layers, with alternating 5, 3 and 5 nm, crystalline, fluid and crystalline phases [Bouwstra; 2001]. Such an arrangement not only ensures low permeability but also some flexibility.

Table 1 Composition of dry stratum corneum, values taken from Jokura (1995) and López (2007).

Dry stratum corneum:

protein: appox. 83 wt%	corneocytes:	mainly keratin
	cornified envelope:	loricrin, involucrin
lipids: approx. 17%	covalently bound: 2 wt%	ceramides, fatty acids
	extracellular lipid matrix: 15 wt%	ceramides (47 wt%), fatty acids (11 wt%), cholesterol (24 wt%), cholesterol esters (18 wt%)

Working with such a complicated system poses a challenge already from the very beginning: the peak assignment, which is necessary in order to make sense of the data on a molecular level. Because the SC is composed of such a variety of molecules it was impossible to unambiguously assign peaks of the PT ssNMR spectra and a simplification of the sample was required.
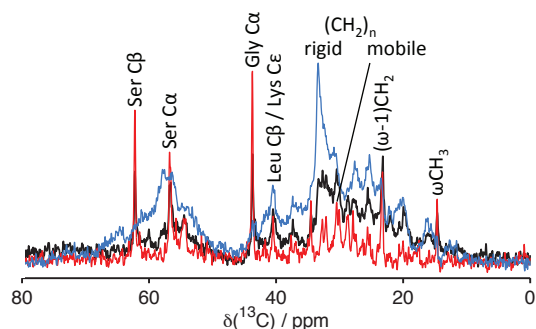
Figure 29 PT ssNMR spectra (DP in black, CP in blue and INEPT in red) and the peak assignment of the most prominent SC peaks.

Extracting the lipids and measuring the corneocytes, with a small fraction of the covalently bound lipids, proved to be helpful, as it facilitated the assignment of the peaks originating from the protein material. Further investigation was carried out on model lipids, where the peaks from cholesterol, ceramides and fatty acids were identified. Comparing the spectra of model lipids and corneocytes with the

intact SC spectra allowed the assignment of all visible peaks. The assignment was further confirmed by performing INEPT experiment with varying delay times, which allowed the identification of CH_3, CH_2 and CH peaks by selectively enhancing CH signals and inverting the CH_2 ones [Elena; 2005]. The result of the peak assignment is available, in the form of a table in Supporting Information of Article IV and, in the form of spectra with labelled peaks, in Article IV. A set of PT ssNMR spectra of intact SC, where the most prominent peaks from proteins and lipids are identified, is presented in Fig. 29.

Subsequently to the peak assignment, a study of the intact SC, under the conditions of varying temperature and water content, was conducted. First, a series of samples equilibrated at different relative humidities has been prepared, in order to provide a picture of the changes of molecular mobility with the changing water content. The acquired spectra are presented in Fig. 30.

It can be observed that at 0 wt% water only a few INEPT peaks, all of which can be assigned to lipids, are visible, pointing to a small fraction of mobile lipids present. This fraction grows as the water content increases until 30 wt%, although a prominent CP $(CH_2)_n$ peak at 33.4 ppm suggests that most lipid chains remain rigid throughout. At water contents higher than 30wt%, the decease of the INEPT $(CH_2)_n$ peak at 30.5 ppm signalizes decrease in the dynamics of the lipid matrix.

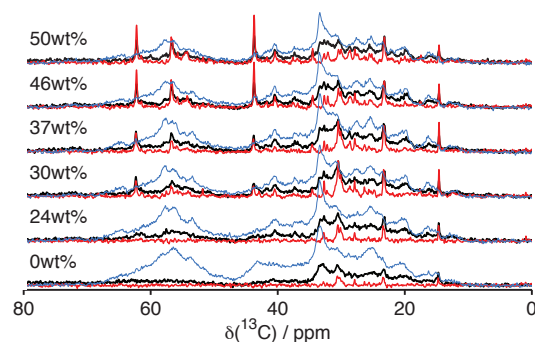Figure 30 PT ssNMR spectra (DP in black, CP in blue and INEPT in red) of SC with increasing water content.

The first protein INEPT peaks become visible only at 30 wt% of water but increase steadily with increasing water content. Those peaks are assigned to glycine and serine, the amino acids enriched in the side chains of the keratin rods, indicating increased mobility in those segments. The leucine/lysine CP peak at 40.5 ppm serves as a marker of rigidity of the main part of the keratin structure, because those amino acids are enriched in the coiled-coil domains of the keratin rods.

The increase in molecular mobility with increasing water content can explain the so-called occlusion effect, which is used to facilitate the transdermal drug delivery [Zhai; 2002]. It is achieved by covering a part of skin, where a drug has been applied, to minimize the drying influence of the air and thus create an environment with higher relative humidity.

Three of the samples, at the water contents of 24, 37 and 50wt%, were chosen for measurements at higher temperatures. A representative series at 37 wt% of water is shown in Fig. 31.
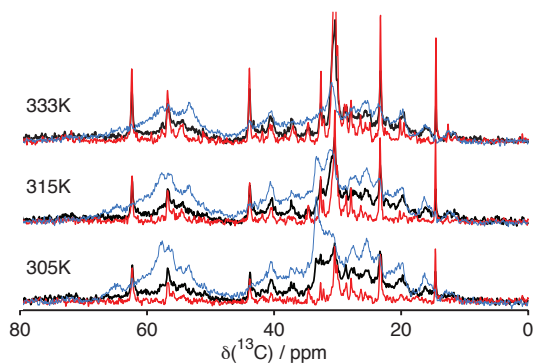
Figure 31 PT ssNMR spectra (DP in black, CP in blue and INEPT in red) of SC with varying temperature at 7 wt% of water.

Interestingly, the effect of increasing temperature is not the same as that of increasing water content. The former seems to affect lipids to a much higher degree, as can be seen by the total disappearance of the CP peak at 33.4 ppm in the measurement at 333 K, signalizing that all lipid chains melt into a liquid crystalline phase. Also the increased intensity of the cholesterol peaks, particularly visible at 12.6 and 40.3 ppm, points to increased mobility of the lipid lamellae. Proteins, on the other hand, seem less dramatically affected by the increasing temperature, with some increase in the mobility of the side chains, but no visible influence on the coiled-coil domains of keratin rods at 37 wt% of water content. Increasing mobility of the coiled-coil domain is only visible at 333 K and 50 wt% water.

Even partial, molecular-scale information, that can be obtained from such a complicated system, is invaluable in interpreting and complementing the data from other experiments that give a more macroscopic description of the system [Björklund; 2010, Sparr; 2009].

Lipid model systems for real problems: amyloid fibrils

The last project I would like to write about deals with the amyloid fibrils and their interactions with cellular membranes.

Fibrillar protein aggregates are implicated in a number of degenerative human diseases [Kirkitadze; 2002], for example the A_β in Alzheimer's, α-synuclein in Parkinson's or a prion protein in Creutzfeldt-Jakob's disease. Thus, a lot of work is being put into understanding the driving forces behind the process of fibril formation [Hamley; 2007], the influence of the cellular environment [Hellstrand; 2010], the role of the aggregates and their intermediates in various diseases [Kirkitadze; 2002] and the possibilities of spreading of the fibrils between infected and healthy cells [Steiner; 2011].
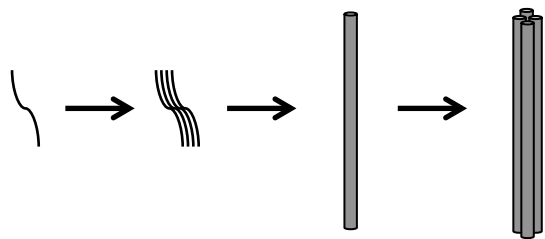
Figure 32 A cartoon of fibril formation.

Fibril formation (Fig. 32) is a process in which unfolded protein molecules assemble into cross-β structures [Hamley; 2007], which form the backbone of long, fibrillar aggregates. Recently, the influence of lipid membranes on the formation of amyloid fibrils has gained much interest [Byström; 2008]. It has been observed that aggregation kinetics are affected by the presence of lipid vesicles and appear to be sensitive to lipid phase behavior and the presence of charged lipids [Hellstrand; 2010, Nasir; 2011]. In the case of Aβ, this interaction seems to slow down the aggregation kinetics [Hellstrand; 2010], while in the study of α-synuclein the opposite has been observed [Nasir; 2011].

It is not yet fully understood how amyloid proteins interact with lipid membranes, nor how this interaction affects the aggregate and membrane properties. One line of thought suggests that the lipid membrane acts as a catalyzing or inhibiting surface for protein aggregation [Murphy; 2007], in which case the lipids themselves are not a part of the process. There are, however, studies that indicate lipid-protein co-aggregation and that the lipids are taken up from a lipid membrane [Sparr; 2004]. The latter is supported by the presence of the lipids in the mature amyloid fibrils [Gellermann; 2005], as well as in plaque aggregates [Gellermann; 2005] and Lewy bodies [Wakabayashi; 2007] from patients with Alzheimer's and Parkinson's diseases, respectively.

α-Synuclein (AS), the protein chosen for this study, is the main component of Lewy bodies, deposits found in the cells of Parkinson's disease patients [Wakabayashi; 2007]. The presence of lipids in the Lewy bodies [Wakabayashi; 2007] and the association of the α-synuclein fibrils with model lipid membranes, shown in a previous study [Grey; 2011], imply protein-lipid interactions, as well as protein-lipid co-aggregation.

The aim of this study was to investigate the possibility of the lipid-protein co-aggregation. Does it occur? Is there selectivity to a certain class of lipids? In the previous study [Grey; 2011], the presence of charged lipids, such as phosphatidylserines (PS) and cardiolipin, provoked the strongest association of the α-synuclein fibrils, suggesting some selectivity.

A mixture of DOPC and DOPS (for molecular structures, see Fig. 18) was used as a model for cellular membrane. DOPC was chosen because phosphatidylcholines (PC) are the most abundant phospholipids in cellular membranes. DOPS represents the PS lipids, which amount to about 20-30 wt% of the inner monolayer of the cellular membrane.

The lipids, in a form of a lamellar phase, as well as the α-synuclein amyloid fibrils, were measured for reference spectra. In the co-aggregation samples, the α-synuclein molecules were allowed to aggregate in the presence of small unilamellar

38

vesicles. To increase the efficiency of PT ssNMR, the aggregates were centrifuged into a more compact form prior to the measurements.

The PT ssNMR spectra of the DOPC/DOPS lamellar phase (Fig. 33a), the co-aggregation sample (Fig. 33b) and the reference α-synuclein fibrils (Fig. 33c) are presented in Fig. 33.

The very presence of the lipid peaks in the spectra of the co-aggregation sample (Fig. 33b) indicates a co-association between the forming fibrils and the lipid vesicles. Small unilamellar vesicles, that were used in the co-aggregation study, would not centrifuge down with the fibrils and thus no lipid peaks would be visible if co-aggregation did not occur. Unfortunately, the decrease of the signal intensity in the headgroup (50-75 ppm) and carbonyl (170-180 ppm) regions of the spectra, probably due to the smaller amount of lipids present in the co-aggregated sample, precludes the possibility to verify the presence of both DOPC and DOPS. It can, however, be observed that one of the DOPC headgroup peaks (right next to the buffer peak) is visible, signalizing the presence of DOPC in the sample.
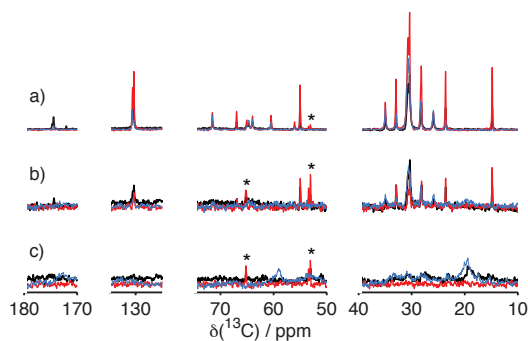

Figure 33 PT ssNMR spectra (DP in black, CP in blue and INEPT in red) of: a) DOPC and DOPS mixture; b) DOPC and DOPS co-aggregated with α-synuclein; c) α-synuclein. The intensity of lipid spectra was divided by four to allow better comparison. The buffer peaks are marked by stars.
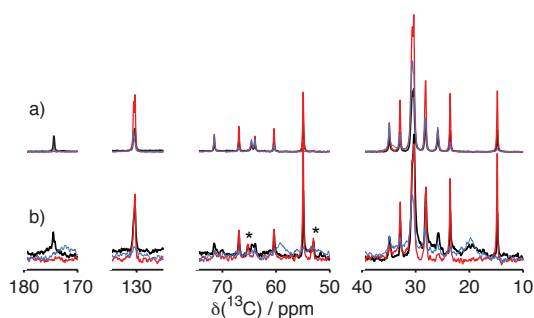

Figure 34 PT ssNMR spectra (DP in black, CP in blue and INEPT in red) of: a) DOPC; b) DOPC co-aggregated with α-synuclein. The intensity of lipid spectra was divided by four to allow better comparison. The buffer peaks are marked by stars.

In order to verify the necessity of the presence of a charged lipid species, analogous experiments were performed with the DOPC vesicles and α-synuclein molecules (Fig. 34).

Also in this case, lipid peaks were observed in the co-aggregation sample (Fig. 34b), signalizing that the fibrils took up the DOPC lipids even in the absence of a charged lipid species.

The phenomenon of lipid-protein co-aggregation has been previously observed as a result of the fibril formation of islet amyloid polypeptide, IAPP [Sparr; 2004], where it led to membrane leakage. *In vivo*, membrane leakage can lead to cell death, possibly explaining the toxicity of the proteins forming amyloid fibrils.

Conclusions

Recently, solid-state NMR has been applied to materials less obviously solid than glass or ceramics, such as the soft matter [Dvinskikh; 2005, Ferreira; 2008, Warschawski; 2000]. Combining different polarization transfer schemes into PT ssNMR led to the development of a tool for investigating the NMR "grey area" that is soft matter at low water contents. The information about molecular mobility that can be gathered with this tool enables the construction of phase diagrams in water regimes that have often been left unexplored previously (Article I). Because the method was designed to combine efficiency with user-friendliness it is suitable for non-NMR specialists to use in their studies as it is comparably robust and easy to set up.

PT ssNMR is also a good probe for real-life systems and biological tissue, where constructing a phase diagram is out of question due to the complicated structure. In such cases, as demonstrated on the stratum corneum (Article IV), it provides a great richness of information on particular components of the system, or a class of components, and their behavior upon changing conditions. The understanding gained through the description of molecular mobility is useful in interpretation and prediction of system properties. Furthermore, PT ssNMR can be used in combination with other experimental techniques to provide a better picture with more details (Article III).

Acknowledgements

I have been very fortunate to get the opportunity to work in a great place and I would like to thank a number of people who made it possible, enjoyable and exhilarating:

- my supervisors, Daniel and Emma, who took me as their PhD student and showed me the amazing world of (solid-state) NMR and its exciting applications. Thank you so much for everything;

- the co-authors of the publications making up the core of this thesis, but also the people with whom I worked on the to-be-written-up projects: thanks for letting me participate in your projects, for sharing your knowledge, experience and enthusiasm;

- Çelen, Diana and Tiago: thank you for reading and commenting on the summary;

- all the past and present members of Physical Chemistry (1), especially the members of the NMR group: thanks for the great atmosphere at work and many memorable coffee breaks and after-works.

Happily, life is not only work and I have been very lucky to meet many lovely people while in Lund (not only chemists!). I would like to acknowledge them now for making my time here fun and keeping me sane: thanks for being such an amazing bunch and sharing your time with me.

Mamie, tacie i Kati dziękuję za bezwarunkową miłość i wsparcie, za to, że zawsze mogę na Was liczyć i że podziwiacie moje „kanapki" pomimo, iż są Wam one zupełnie nieprzydatne.

Renaud, mon chéri, si tu n'existais pas dis-moi pour qui j'existerais? Merci.

References

- **Alemany L. B.**, Grant D. M., Pugmire R. J., Alger T. D., Zilm K. W., *"Cross polarization and magic angle sample spinning NMR spectra of model organic compounds. 1. Highly protonated molecules"*, J. Am. Chem. Soc. **1983**, *105*, 2133-2141

- **Alonso B.**, Massiot D., *"Multi-scale NMR characterization of mesostructured materials using ^1H – ^{13}C through-bond polarization transfer, fast MAS, and ^1H spin diffusion"*, J. Magn. Res. **2003**, *163*, 347-352

- **Anchordoguy T. J.**, Rudolph A. S., Carpenter J. F., Crowe J. H., *"Modes of interaction of cryoprotectants with membrane phospholipids during freezing"*, Cryobiology **1987**, *24*, 324-331

- **Arnold J. T.**, Dharmatti S. S., Packard M. E., *"Chemical effects on nuclear induction signals from organic compounds"*, J. Chem. Phys. **1951**, *19*, 507

- **Atkins P.**, de Paula J., *"Atkins' Physical Chemistry"*, 8th edition, Oxford University Press **2006**

- **Bennett A. E.**, Rienstra C. M., Auger M., Lakshmi K. V., Griffin R. G., *"Heteronuclear decoupling in rotating solids"*, J. Chem. Phys. **1995**, *103(16)*, 6951-6958

- **Björklund S.**, Engblom J., Thuresson K., Sparr E., *A water gradient can be used to regulate drug transport across skin"*, J. Control. Release **2010**, *143*, 191-200

- **Bouwstra J. A.**, Gooris G. S., Dubbelaar F. E. R., Ponec M., *"Phase behavior of lipid mixtures based on human ceramides: coexistence of crystalline and liquid phases"*, J. Lip. Res. **2001**, *42*, 1759-1770

- **Bussy U.**, Thibaudeau C., Thomas F., Desmurs J.-R., Jamin E., Remaud G. S., Silvestre V., Akoka S., *"Isotropic finger-printing of active pharmaceutical ingredients by ^{13}C NMR and polarization transfer techniques as a tool to fight against counterfeiting"*, Talanta **2011**, *85*, 1909-1914

- **Byström R.**, Aisenbrey C., Borowik T., Bokvist M., Lindström F., Sani M.-A., Olofsson A., Gröbner G., *"Disordered proteins: biological membranes as two-dimensional aggregation matrices"*, Cell Biochem. Biophys. **2008**, *52*, 175-189

- **Costa-Balogh F. O.**, Wennerström H., Wadsö L., Sparr E., *"How small polar molecules protect membrane systems against osmotic stress: The urea-water-phospholipid system"*, J. Phys. Chem. B **2006**, *110*, 23845-23852

- **Dvinskikh S. V.**, Castro V., Sandström D., *"Efficient solid-state NMR methods for measuring heteronuclear dipolar couplings in unoriented lipid membrane systems"*, Phys. Chem. Chem. Phys. **2005**, *7*, 607-613

- **Earl W. L.**, VanderHart D. L., *"Observations in solid polyethylenes by carbon-13 nuclear magnetic resonance with magic angle sample spinning"*, Macromolecules **1979**, *12*, 762-767

- **Elena B.**, Lesage A., Steuernagel S., Böckmann A., Emsley L., *"Proton to carbon-13 INEPT in solid-state NMR spectroscopy"*, J. Am. Chem. Soc. **2005**, *127*, 17296-17302

- **Ericsson C. A.**, Ericsson L. C., Kocherbitov V., Söderman O., Ulvenlund S., *"Thermotropic phase behavior of long-chain alkylmaltosides"*, Phys. Chem. Chem. Phys. **2005**, *7*, 2970-2977

- **Evans D. F.**, Wennerström H., *"The colloidal domain: where physics, chemistry, biology and technology meet"*, 2nd edition, Wiley-VCH **1999**

- **Ferreira T. M.**, Medronho B., Martin R. W., Topgaard D., *"Segmental order parameters in a non-ionic surfactant lamellar phase studies with 1H-13C solid-state NMR"*, Phys. Chem. Chem. Phys. **2008**, *10*, 6033-6038

- **Forslind B.**, Lindberg M., *"Structure and function of the skin barrier: An introduction"*, Skin, hair and nails: Structure and function **2004**, Marcel Dekker, 11-23

- **Gellermann G. P.**, Appel T. R., Tennert A., Radestock A., Hortschansky P, Schroeckh V., Leisner C., Lütkepohl T., Shtrasburg S., Röcken C., Pras M., Linke R. P., Diekmann S., Fändrich M., *"Raft lipids as common components of human extracellular amyloid fibrils"*, PNAS **2005**, *102*, 6297-6302

- **Genix A.-C.**, Lauprêtre F., *"Subglass and glass transitions of poly(di-n-alkylitaconate)s with various side-chain lengths: Solid-state NMR investigation"*, Macromol. **2006**, *39*, 7313-7323

- **Grey M.**, Linse S., Nilsson H., Brundin P., Sparr E., *"Membrane interaction of a-synuclein in different aggregation states"*, J. Parkinson's Disease **2011**, *1*, 359-371

- **Halle B.**, Wennerström H., *"Interpretation of magnetic resonance data from water nuclei in heterogenous systems"*, J. Chem. Phys. **1981**, *75(4)*, 1928-1943

- **Hamley I. W.**, *"Peptide fibrillization"*, Angew. Chem. Int. **2007**, *46*, 8128-8147

- **Harris R. K.**, *"Nuclear magnetic resonance spectroscopy"*, Longman Group UK Limited **1986**

- **Harris R. K.**, *"NMR studies of organic polymorphs & solvates"*, Analyst **2006**, *131*, 351-373

- **Hellstrand E.**, Sparr E., Linse S., *"Retardation of Aβ fibril formation by phospholipid vesicles depends on membrane phase behavior"*, Biophys. J. **2010**, *98*, 2206-2214

- **Herzfeld J.**, Berger A. E., *"Sideband intensities in NMR spectra of samples spinning at the magic angle"*, J. Chem. Phys. **1980**, *72*, 6021-6030

- **Hirschinger J.**, *"A simple analytical model to describe dynamic magic-angle spinning experiments"*, Conc. Magn. Reson. A **2006**, *28*, 307-320

- **Hore P. J.**, *"Nuclear magnetic resonance"*, Oxford University Press **1995**

- **Jokura Y.**, Ishikawa S., Tokuda H., Imakowa G., „*Molecular analysis of elastic properties of the stratum corneum by solid-state 13C-nuclear magnetic resonance spectroscopy*", J. Invest. Derm. **1995**, *104*, 806-812

- **Kirkitadze M. D.**, Bitan G., Teplow D. B., *"Paradigm shifts in Alzheimer's disease and other neurodegenerative disorders: The emerging role of oligomeric assemblies"*, J. Neaurosci. Res. **2002**, *69*, 567-577

- **Kocherbitov V.**, Söderman O., *"Glassy crystalline state and water sorption of alkyl maltosides"*, Langmuir **2004**, *20*, 3056-3061

- **Laws D. D.**, Bitter H.-M. L., Jerschow A., *"Solid-state NMR spectroscopic methods in chemistry"*, Angew. Chem. Int. Ed. **2002**, *41*, 3096-3129

46

- **Levitt M. H.**, *"Spin dynamics. Basics of nuclear magnetic resonance"*, John Wiley & Sons, Ltd **2008**

- **López O.**, Cócera M., Wertz P. W., López-Iglesias C., de la Maza A., *"New arrangement of proteins and lipids in the stratum corneum cornified envelope"*, Bioch. Biophys. Acta **2007**, *1768*, 521-529

- **Markowa N.**, Sparr E., Wadsö L., Wennerström H., *"A calorimetric study of phospholipid hydration. Simultaneous monitoring of enthalpy and free energy"*, J. Phys. Chem. B **2000**, *104*, 8053-8060

- **Marstein S.**, Jellum E., Eldjarn L., *"The concentration of pyroglutamic acid (2-pyrrolidone-5-carboxylic acid) in normal and psoriatic epidermis, determined on a microgram scale by gas chromatography"*, Clin. Chim. Acta **1973**, *49*, 389-395

- **Morris G. A.**, Freeman R., *"Enhancement of nuclear magnetic resonance signals by polarization transfer"*, J. Am. Chem. Soc. **1979**, *101*, 760-762

- **Murphy R. M.**, *"Kinetics of amyloid formation and membrane interaction with amyloidogenic proteins"*, Biochim. Biophys. Acta **2007**, *1768*, 1923-1934

- **Nasir, I.**, *"Kinetic and surface properties of a-synuclein: Investigating the difference between pure peptide and phospholipid including aggregates"*, Master thesis **2011**

- **Pines A.**, Gibby M. G., Waugh J. S., *"Proton-enhanced nuclear induction spectroscopy. A method for high resolution NMR of dilute spins in solids"*, J. Chem. Phys. **1972**, *56*, 1776-1777

- **Ramløv H.**, *"Aspects of natural cold tolerance in ectothermic animals"*, Hum. Reprod. **2000**, *15*, 26-46

- **Rawlings A. V.**, *"Trends in stratum corneum research and the management of dry skin conditions"*, Int. J. Cosmet. Sci. **2003**, *25*, 63-95

- **Rawlings A. V.**, Harding C. R., *"Moisturization and skin barrier function"*, Dermatol. Therapy **2004**, *17*, 43-48

- **Robert E.**, Whittington A., Fayon F., Pichavant M., Massiot D., *"Structural characterization of water-bearing silicate and aluminosilicate glasses by high-resolution solid-state NMR"*, Chem. Geol. **2001**, *174*, 291-305

- **Sparr E.**, Engel M. F. M., Sakharov D. V., Sprong M., Jacobs J., de Kruijff B., Höppener J. W. M., Killian J. A., *"Islet amyloid polypeptide-induced membrane leakage involves uptake of lipids by forming amyloid fibers"*, FEBS Letters **2004**, *577*, 117-120

- **Sparr E.**, Åberg C., Nilsson P., Wennerström H., *"Diffusional transport in responding lipid membranes"*, Soft Matter **2009**, *5*, 3225-3233

- **Steiner J. A.**, Angot E., Brundin P., *"A deadly spread: cellular mechanisms of a-synuclein transfer"*, Cell Death Differ. **2011**, *18*, 1425-1433

- **Storey K. B.**, Storey J. M., *"Freeze tolerance and intolerance as strategies of winter survival in terrestrially-hibernating amphibians"*, Comp. Biochem. Physiol. **1986**, *83A*, 613-617

- **VanderHart D. L.**, Earl W. L., Garroway A. N., *"Resolution in 13C NMR of organic solids using high-power proton decoupling and magic-angle sample spinning"*, J. Magn. Res. **1981**, *44*, 361-401

- **Wakabayashi K.**, Tanji K., Mori F., Takahashi H., *"The Lewy body in Parkinson's disease: Molecules implicated in the formation and degradation of the a-synuclein aggregates"*, Neuropathology **2007**, *27*, 494-506

- **Warschawski D.**, Devaux P. F., *"Polarization transfer in lipid membranes"*, J. Magn. Res. **2000**, *145*, 367-372

- **Westh P.**, *"Unilamellar DMPC vesicles in aqueous glycerol: preferential interactions and thermochemistry"*, Biophys. J. **2003**, *84*, 341-349

- **Yancey P. H.**, Clark M. E., Hand S. C., Bowlus R. D., Somero G. N., *"Living with water stress: evolution of osmolyte systems"*, Science **1982**, *217*, 1214-1222

- **Zhai H.**, Maibach H. I., *"Occlusion vs. skin barrier function"*, Skin Res. Technol. **2002**, *8*, 1-6